Image Analysis Methods For Additive Manufacturing Applications

Jayanth Ramakrishna Yogendra

GKN AEROSPACE

UNIVERSITY WEST

Summary

There is an upsurge of research interest on Ni-based superalloys additively manufactured (AM) in aerospace sectors. However, achieving the accuracy and quality of the AM part is a challenging task because it is a process of adding material layer by layer with different process parameters. Hence, defects can be observed, and these defects have a detrimental effect on the mechanical properties of the material. Also, AM materials commonly portray a columnar grain structure which also makes it difficult to determine the average grain size because while using the commonly used intercept method, the grain boundaries do not intercept to the test line appropriately. It is important to measure the defects and grain size before performing mechanical testing on the material. Defect measurement and grain size measurements are usually measured manually which results in longer lead time. This work is addressed towards testing recipes in the automated image analysis software to optimize the lead time with good accuracy.

Haynes 282, a γ' strengthened superalloy is used in this work. It was assumed that 1,5mm of material from the surface will be machined away so defects had to be measured in this region of interest. The image analysis tools used to test its potentials are MIPAR and ImageJ. Initially, five images in MIPAR and Image J were tested keeping the manual measurements as a benchmark. From this part, it was concluded that metallography and image quality play an important role in the automated measurement. Also, basic Image J software cannot give the measurements of lack of fusion in terms of caliper diameter (longest measurable diameter). Hence, MIPAR was chosen for the application because it was more promising. In the next part, 15 samples were used with manual measurements from a stitched sample and batch processing with MIPAR. The total caliper diameter results were plotted to compare manual measurements and MIPAR. It was observed that scratches were measured as lack of fusion defects at few instances by MIPAR which were further refined using a post-processing function. The defect density results were plotted and compared as well. Due to the difference in calculation of region of interest, the difference in results was observed.

To perform the grain size measurement, Haynes 282 was used in HIP and heat treated condition, achieving equiaxed grains. The etchant should be appropriate to reveal the grains.

Hence four different etchants were used in this study hydrogen peroxide+HCl, Kallings (electro etch), Kallings(swab) and diluted oxalic acid. This measurement was performed on the material which was cut along the build direction as well as 90° to the growth direction. Since there is no standard for additively manufactured material yet, the results were tested with hall-petch equation to be convinced of the results obtained. It was observed that MIPAR recipe portrayed good results. The results of manual measurements and MIPAR measurements were plotted and compared. It was observed that Hydrogen peroxide and Kallings (swab) showed the grains evidently but twin boundaries were revealed as well. MIPAR calculated the twin boundaries as grains so it over calculated than manual measurements. Kallings (electro etch) and diluted oxalic acid did not reveal the grains so it was difficult for MIPAR to identify the grains.

Acknowledgement

Affirmation

This master degree report, Image Analysis methods for Additive Manufacturing Applications, was written as part of the master degree work needed to obtain a Master of Science with specialization in Advanced manufacturing engineering technology degree at University West. All material in this report, that is not my own, is clearly identified and used in an appropriate and correct way. The main part of the work included in this degree project has not previously been published or used for obtaining another degree.

18/08/2020

_____   _____

Signature by the author   Date

Jayanth Ramakrishna Yogendra

Contents

Appendices

A.   APPENDIX

B.   APPENDIX

Symbols and glossary

AM   Additive Manufacturing

PBF   Powder Bed Fusion

DED   Directed Energy Deposition

LOM   Light Optical Microscope

SEM   Scanning Electron Microscope

TEM   Transmission Electron Microscope

MC   Metal Carbide

ROI   Region of Interest

HIP   Hot Isostatic Pressing.

HT   Heat Treatment

Ni-based   Nickel based

3D   3 Dimensional

CAD   Computer Aided Drawing

List of Figures

1   Introduction

There has been an upsurge in additive manufacturing of Ni – based superalloys in the aviation industry. AM is a process of building layer over another layer of material to achieve the final product according the CAD model input to the 3D printing machine. Although it has many advantages over subtractive manufacturing, yet there exists few concerns that should be addressed in order to apply it on the real time applications in regular basis.

Figure 1 shows a logical flowchart of additive manufacturing. Initially we have the process engineers performing different design of experiments for deciding the process
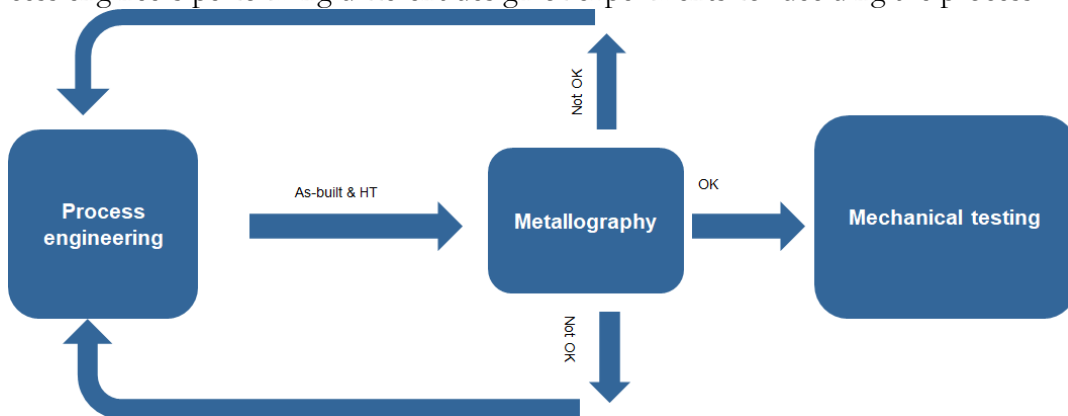
Figure 1 - Flowchart of typical Additive manufacturing

parameters to manufacture the material. It is further sent to the metallography group for evaluation. Material preparation and metallography steps such as cutting, moulding, grinding, polishing, microscopic evaluation is performed to check if the quality of the material is in the range of acceptance. If it is in an acceptable range, it is forwarded to the mechanical testing team to perform mechanical testing. In case the material is not within the prerequisite requirements, the material is sent back to the process engineering team for modifying the process parameters. During the testing by the metallography team, it takes higher lead time as it is measured manually. Hence to reduce the lead time while not sacrificing the quality of the measurements, automated image analysis techniques is necessary.

1.1 Objective

1. To determine the best software for defect analysis of additively manufactured components while testing the current recipes for accuracy using image analysis.

2. To determine a suitable etchant and a procedure for grain size measurement of additive manufacturing materials using image analysis.

2   Background

2.1 Gas Turbines

Gas turbines are utilized in many applications. It has been a valuable part of the aviation industry since 1900 by dominating the power generation and aero-engine industries [1]. The operating temperature of gas turbines is very high at which steels cannot resist and tend to soften. Electric power is supplied by the gas turbine to propel large machinery like aircraft. A gas turbine consists of fan, low-pressure compressor, high-pressure compressor, combustion chamber, high-pressure turbine and low-pressure turbine. The inlet air is compressed in the compressor so that the pressure of the air is increased. The compressed air is mixed with fuel and ignited after it enters the combustion chamber. The output gases are directed over the turbine blades which makes the turbine to rotate finally giving power to the compressor mechanically. There is an increase in the thrust as the hot gases are passed through the nozzle [2]. This demands a heat resistant material because of the high temperature change it experiences. Hence, Ni-based superalloy is used as they are heat resistant materials [2]. A typical gas turbine schematic is observed in Figure 2
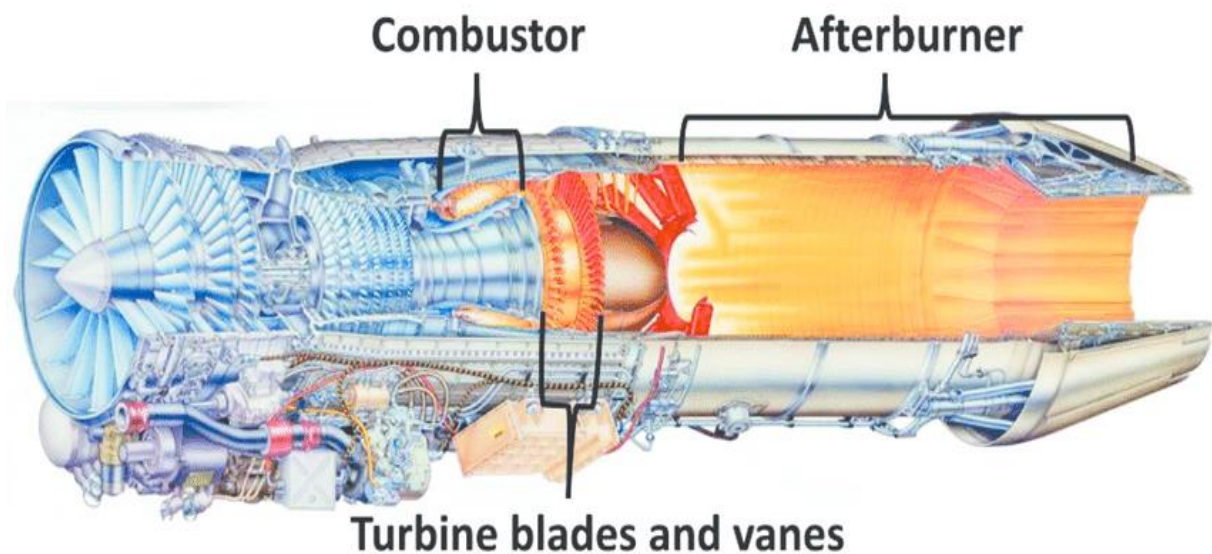
Figure 2 – Schematic representation of the gas turbine [1].

2.2 Ni-based Superalloy

Based on strengthening mechanisms, superalloys is classified into Ni-based (solid solution strengthening), Ni-iron based (precipitation strengthening) and Co-based (oxide dispersion strengthening) [3]. A Ni-based superalloy is the most widely used material for applications experiencing high stress and high temperature. They offer uniform properties, fewer defects and less elemental segregation which in return helps to improve mechanical properties. They contain a lot of alloying elements because they involve precipitation of intermetallic phases such as gamma prime (γ'), gamma double prime (γ") and carbides. These precipitation phases offer the material with superior strength, high resistance to oxidation, corrosion and the creep properties from these phases [3]. Many different heat treatments are performed for the sake of stress-relieving, homogenization and annealing. The properties are optimized by heat treatments.

The composition of the superalloys is determined by the alloying elements used. The role of alloying elements is explained in Table 2.

Table 1- Role of alloying elements

Element	Range in Fe-Ni and Ni-base alloys (wt%)	Effect
Cr	2-25	Oxidation and hot corrosion resistance, carbides, solution hardening
Mo,W	0-12	Carbides,solution hardening
Al	0-6	Precipitation hardening and oxidation resistance
Ti	0-6	Precipitation hardening and carbides
Co	0-20	Affects amount of precipitate

Ni	-	Stabilizes austeninte and forms hardening precipitates
Nb	0-5	Carbides, solution hardening, precipitation hardening
Ta	0-12	Carbides, solution hardening, oxidation resistance

2.3 Additive Manufacturing

Additive manufacturing is defined as manufacturing a product with layer by layer deposition of material as per the data obtained from the 3D CAD model using a 3D printing machine. Complex shapes and custom made shapes can be achieved by additive manufacturing method than in the conventional methods. It is not more particularly used for prototyping technology, but it is also used for the production of components used in extreme conditions. It exhibits a trend for the upcoming manufacturing technology development and is expected to play an increasingly important role in high-end product manufacturing and to promote global economic development [4]. In additive manufacturing, a CAD model is initially designed with the desired dimensions and fed into the 3D printing equipment. The equipment will process it and create layering for the 3D CAD model according to the thickness required for each layer while manufacturing. The product is manufactured layer by layer. There are many types of additive manufacturing such as powder bed fusion(electron beam- powder bed fusion and laser- powder bed fusion), directed energy deposition(powder and wire), binder jetting and sheet lamination. The main processes include -

➢ Powder Bed Fusion(PBF) –

PBF is a type of process in which an energy source such as electron beam or a laser beam is used to solidify the required regions according to the 3D CAD model by spreading powder all over the bed [5]. A rake is used to spread powder and rakes away powder according to the layer thickness needed per layer. After the sintering of one layer is done, the unsintered particles are eliminated and sent back for re-use. After each layer is sintered, the bed moves lower and the next

layer is sintered according to the 3D model. The schematic of the powder bed fusion is shown in Figure 3
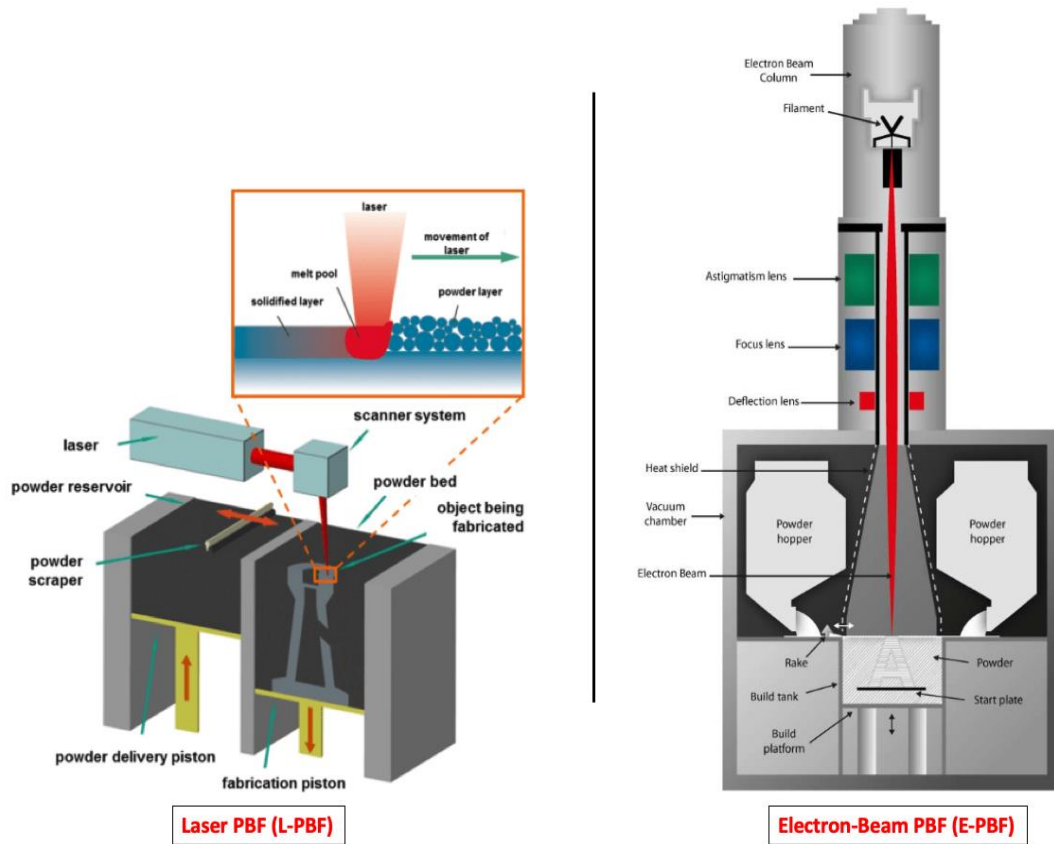
Figure 3 – Schematic explanation of the PBF process with Laser and Electron beam as the energy source [5].

➢ Directed energy deposition (DED)-

DED as shown in Figure 4 is a type of process in which an energy source such as a laser or electron beam is used to focus on the required area to be solidified on the material. It creates a melt pool and the powder or wire is fed into the melt pool that solidifies on the base plate. The same procedure is repeated layer by layer finally achieving the required object according to the 3D CAD model. This
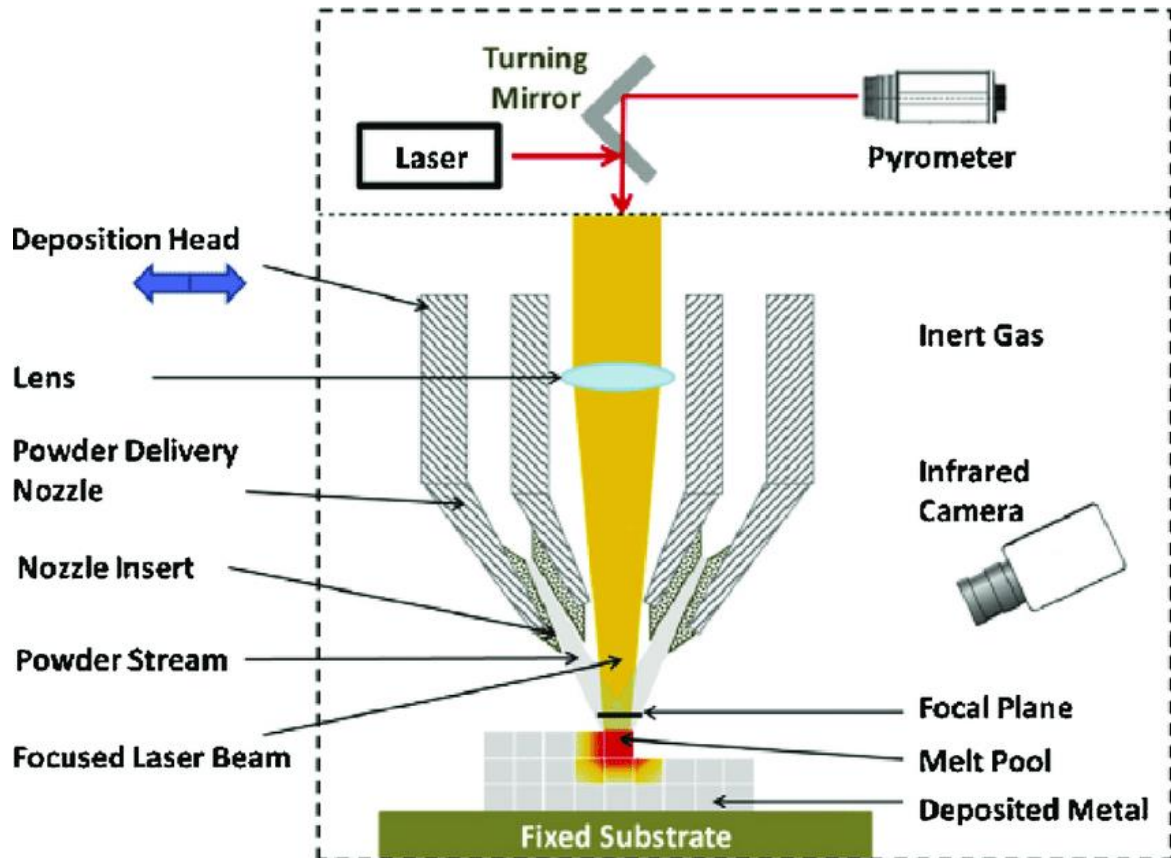
Figure 4 – Schematic explanation of DED [36].

process has the ability to build the required parts from scratch but it is commonly used to repair work of damaged parts.

➢ Binder Jetting (BJ)

Binder Jetting is a type of process in which a liquid binding agent is chosen to deposit the powder particles. Initially metal powder is spread over the build platform and the liquid binder is dropped into the powder to deposit the layer with the print head [6]. The building platform lowers as per the required layer thickness and the same procedure is continued until the final product has been achieved. The product is manufactured according to the 3D CAD model input to the machine. The schematic of the process is shown in Figure 5.
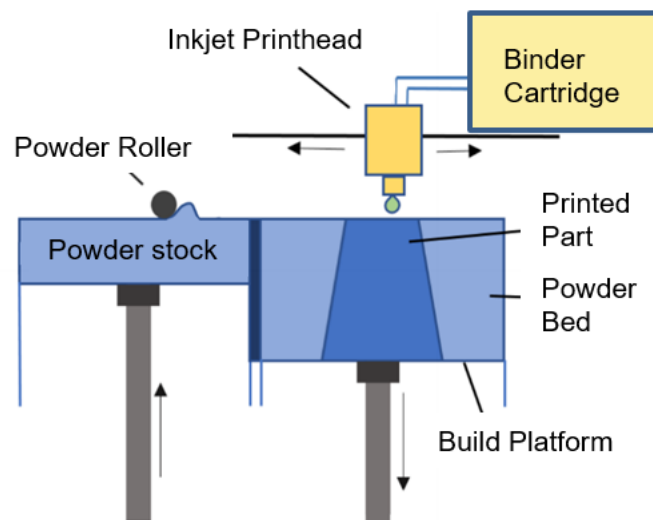
Figure 5 – Schematic of Binder jetting [6]

2.4 Microstructure and Phases

The additively manufactured metals have structures and microstructures which are different from that of cast or wrought because of the directional solidification and rapid cooling [7]. The growth of the microstructure is generally predicted with the help of

G*R ratio as shown in Figure 6. Columnar grains are achieved with higher temperature gradient and low cooling rates while on the other hand equiaxed growth of dendrites
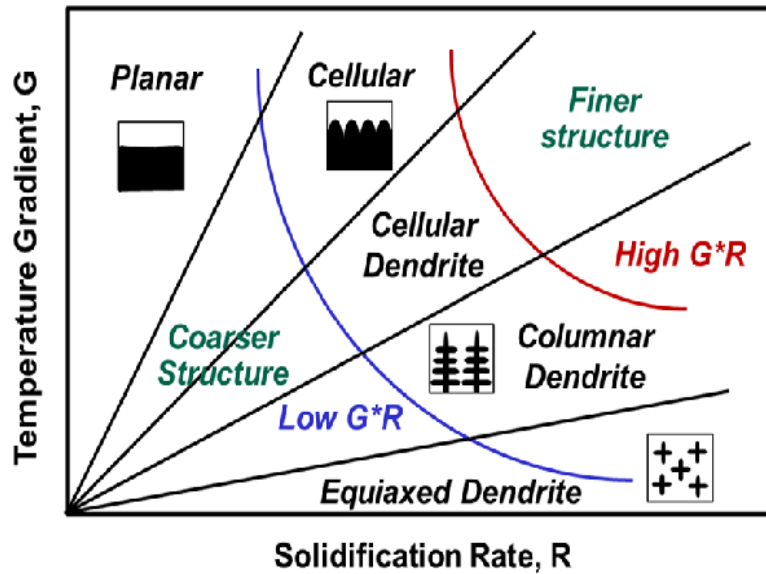
Figure 6 - The effect of G and R on the solidification [37]

is achieved with low thermal gradient and high cooling rates [6] as observed in the Figure 7. The microstructures generally achieved by AM are anisotropic microstructure with elongated columnar grains along the build direction.
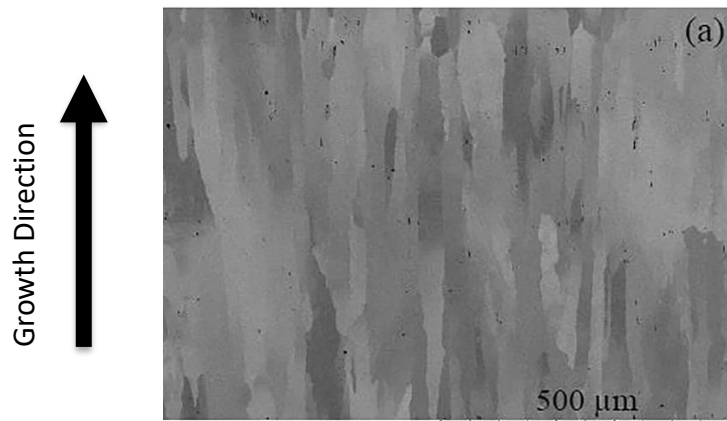
Figure 7 – Columnar grain structure in Additive Manufacturing

During the solidification process, different phases are formed. When compared to Cobalt-base alloys, Iron-nickel base and nickel-base superalloys offer a pronounced evolution of microstructure. They have FCC structure among which the most commonly found are as follows

➢ γ matrix - It is a non-magnetic phase with a continuous matrix containing elements such as iron, molybdenum, cobalt and tungsten [8]. Nickel doesn't portray low diffusivity or exceptional high elastic modulus.

➢ γ' phase – It is formed along long grain boundaries in the cast and wrought alloys helping to improve the creep-rupture properties [8]. It is formed by the heat treatment performed on the material or by the service operation. The advantages of this phase are that the coherence with the γ phase matrix gives a good stability and low surface energy. This phase provides high-temperature strength and creep resistance to the superalloys [9]. The volume fraction of γ' gives strength of the alloy.

➢ γ'' phase –It exhibits higher coherency strains in the matrix because of the higher degree of mismatch as it confers higher strength but lower thermal stability and the precipitation is slower compare to the γ' phase strengthening [10]. they give a lot of strength at the low-to-intermediate temperature but it becomes unstable above 649 approximately [4].

➢ Carbides – They are incoherent to the matrix and are found on the grain boundaries intergranularly [3]. There are many types of carbides, MC carbides decomposes and generates other carbides such as M23C6 and M6C at grain boundaries during heat treatment and service [8]. Eutectic MC Carbides and M23C6 particles present at the grain boundaries inhibit grain boundary mitigation during deformation helping to enhance the fatigue performance but continuous carbide chain formed at grain boundary leads to propagating cracks resulting in failure [10].

Reactions are as follows [10] –

1. $MC + \gamma = M_{23}C_6 + \gamma'$
2. $MC + \gamma = M_6C + \gamma'$

Table 2 - Phases in superalloys [8]

Phase	Crystal structure	Comments
γ' Ni_3Al $Ni_3(Al, Ti)$	FCC(ordered $L1_2$)	Principle strengthening phase. γ' was spherical in some previously developed Ni-base alloys but they are apparently cuboidal in the newly developed Ni-base superalloys
MN TiC	Cubic	The composition varies, it appears as globular, irregularly shaped particles
$M_{23}C_6$ $Cr_{23}C_6$	FCC	It can precipitate in form of globules, platelets, and cells generally found at the grain boundaries
M_6C Fe_3Mo_3C	FCC	
M_3B_2 Ta_3B_2 V_3B_2 Nb_3B_2	tetragonal	Boride and carbides look similar but the preferential carbide etchants does not affect them.

2.5 Applications

2.5.1 Haynes 282

In the present generation, the market demands an irreplaceability of Ni-based superalloy with applications experiencing extreme environments. Hence, there was a constant attempt to create advancement to meet the new demands [9]. In the year 2005 Haynes international developed a corrosion-resistant and high creep strength Ni-based superalloy to replace waspalloy for different components in the aero-engine industry [3] . It overcomes the disadvantage of waspalloy not being weldable and some temperature limitations created by Inconel 718 and Waspaloy.

It is classified as a wrought, gamma prime strengthened superalloy. It has a good creep strength at the high-temperature range of 1200 to 1650°C although it has a significantly low volume fraction of the strengthening gamma prime phase [11]. It provides an improvement in fabricability and resistance to strain-age cracking which is the usual problem observed in this class of alloys [11] . The mechanical properties are controlled by heat treatments with the solutionizing and ageing process having a standard of solution treatment at 1121-1149 °F and two-stage age-hardening treatment at 1010°F for 2hours + 780°C for 8 hours [9]. Haynes 282 show sensitivity to heat treatment parameters resulting in different morphologies of carbides at grain boundaries and bimodal precipitation of gamma prime precipitates [3] . The gamma prime precipitation is suppressed during rapid quenching [3].

2.6 Defects

Defects are an imperfection created in the material during solidification. It acts as a detrimental effect on the mechanical properties of the additively manufactured materials. Different types of defects commonly found in additively manufactured parts are as follows.

> ➤ Lack of fusion – This type of defect occurs when there is a lack of required heat for the adhesion of the layers. This defect is formed because the metal powders are not fully melted to deposit over the previous layer [12]. They are found between two layers and are commonly observed in additively manufactured applications because of the layer by layer building process observed. They show detrimental effects on the components exposed to cyclic loads [13]. The surface tends to have roughness at the location of defects which will not allow the molten metal to flow appropriately.

> ➤ Porosity- This type of defect occurs in two types such as round pores and irregular pores. The round pores are caused because of the gas trapped in the pore. They contribute less to the material failure because only pores above a certain level of acceptance are considered as a threat. There is a level of acceptance for porosity measurement which is assumed after performing the tests many times. The irregular pores are more of a threat because they contribute to increasing the concentration of stress leading to material failure.

➢ Cracks – This defect occurs usually when strain exceeds the material ability to deform. The precipitation strengthened materials have chances of cracking during heat treatment due to the dip in ductility and rise in hardness when a certain extent of precipitates is reached [14]. Residual stress occurs due to the non-uniform temperature gradient. It influences the component's dimensional and geometrical accuracy depending on the magnitude for material's strength. These residual stresses are released as the crack expands.

2.7 Image Analysis

Image analysis is a rich description of something that can depict a piece of important information in the form of pictures, drawings, documents and animation. It is usually represented by a 2D array f(x,y) in which x and y are the coordinate points in a 2D space [15]. Each basic unit in a 2D image is called as a pixel in case of a 3D image, it is called a voxel. To develop an image application, a basic theory of mathematics, optics etc is required. There are three types of image engineering as shown in Figure 8.
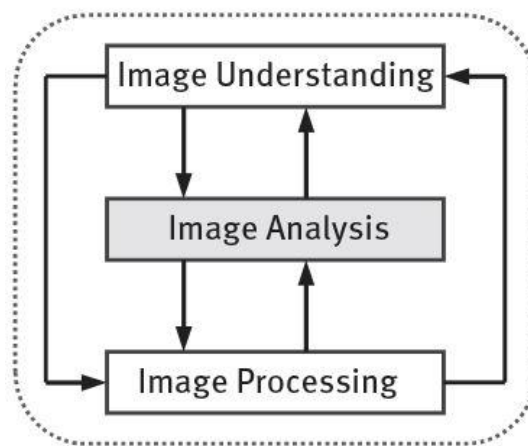

**Figure 8 - Methods in Image analysis
[15].**

Image analysis is performed to analyze the image and extract some required data to explain the characteristics of an image. An output data results are obtained after detecting, extracting, representing, describing and measuring the image. From the Figure 9, it is schematically explained how an image is processed and converted into required result by detecting the image and equated using equations

$$(x-5)^2 + (y-7)^2 = 4^2$$
$$\sigma = 0.3$$

$\leftrightarrow$ Circle

(a) (b) (c) (d)
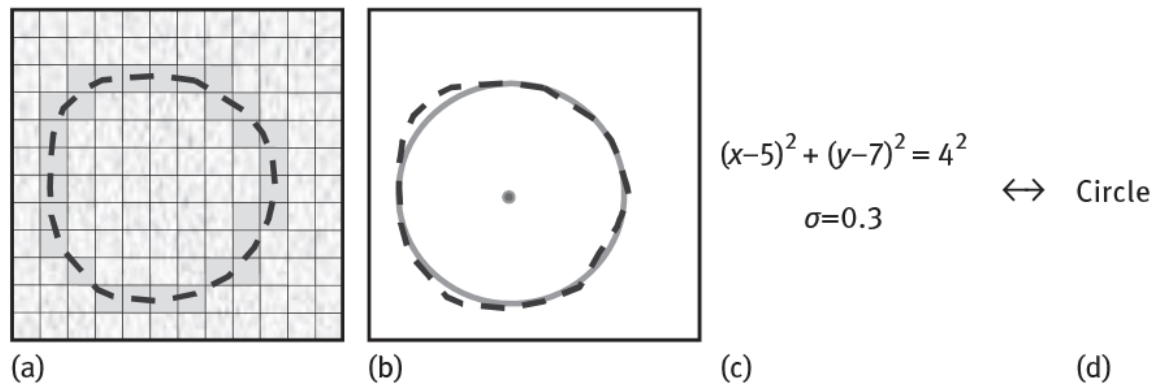
Figure 9 - Symbolic expression of Image processing [15].

In manual measurements, the accuracy, time and reproducibility become a fatigue for the operator because of the human factor leading to operator fatigue. Image analysis is considered because it reduces operator fatigue. It becomes important for the usage of an automated device because the material samples being tested are not homogeneous [16]. By using automated methods, a greater number of samples can be tested with more accuracy and quality. Some important goals in image analysis is to get a refined understanding of the structured data to extract material characteristics, large data volumes to be analyzed efficiently, improve the materials properties, to observe the material properties and keep track of the quality with material comparison, to enhance the production process and keep the physical properties constant. Sample preparation plays a very important role in image analysis because the sample should be mounted and polished appropriately to obtain good images. It is important to obtain good images for quality and precision of the automatic image analysis process because a low-quality image cannot be processed and detected by the software. Edge detection is a major thing to be concerned because there is a lot of change in greyscale levels [15]. Generally there exists an inaccuracy in the measurement of particles smaller than 2 μm approximately when observed in a LOM [16].

Defect analysis is calculated manually in the same software that is used for the optical microscope. The diameter of pores and the length of the cracks and lack of fusion is measured utilizing the measurement tools available. Pores measuring less than a particular measurement such as 50 μm is neglected. After the calculation, the results can be sorted in a statistical table. The average grain size is measured to predict the final mechanical properties.

2.7.1 **Basic procedures** [17]:

➢ Comparison procedure – As the name suggests they are compared to some charts containing a plate with different standards. This method holds good for totally recrystallized materials with equiaxed grains

➢ Planimetric procedure – The number of grains is supposed to be counted in a particular area of interest. This method is slow and less popular because accuracy cannot be achieved. Sometimes it happens that some part of the grain is inside the Region of Interest (ROI) circle, in such cases the operator has to mark off the grains they count. For image analysis, this method holds good [18]. The equation (a) used for the calculation is [17]

N=2 $^{G-1}$ ------------ (a)

Where

N is the number of grains per unit at 100X magnification

G is the ASTM grain size number

➢ Intercept procedure – This method is a comparatively faster way to perform manual measurements. The number of grains or grain boundary intersection which is intercepted by a test line per unit length is used to measure the linear intercept length. They are utilized for elongated grains. This method is performed by either counting grain boundary intersection P or grains intercepted, N. The P count divided by the true lines length, LT, which is the line length divided by the magnification, L/M. This results in PL, the number of intersections per unit length. The reciprocal of PL is the mean linear intercept length, L3 [19]. The empirical equation (b) is

G = (-6.6457 log L$_3$) – 3.298 ------------ (b)

Systematic manual point count [20]

1. Estimate the area percent of feature in a metallographic section of interest manually
2. Select the grit size (PT)
3. Superimpose the grid in a microscope with a suitable magnification such that the size of the features of interest is almost one half of the spacing between grid points.
4. Select a statistical precision (%RA) desired for the measurements.
5. Obtain an estimate of the number of fields (n) necessary to obtain the desired degree of precision.
6. Determine the spacing between fields that will form an equally spaced array covering most of the area without overlap.
7. Determine the number of turns required on the stage translation knobs to move the stage from one position to another.
8. Measure the number of grid points (Pi) falling within the feature of interest.
9. Calculate the average points per field (*Pp*)

2.7.2. Automatic Image analysis method

The automatic image analysis demands high-quality metallographic preparation of the sample because the quality of the image is directly related to the accuracy of the analysis. Edge detection is a very prime task because of the difference in the threshold.

The systematic approach followed in an automated image analysis method is [15] :

➢ Image acquisition – To perform image analysis, a piece of equipment is required to obtain good images such as LOM, SEM, and TEM.

➢ Preprocessing – While acquiring images from the microscope, few distortions are created. All the distortion is optimized.

➢ Image restoration – Applying filters on the image so that there will be background correction, reduction in noise and other kinds of distortion.

➢ Image segmentation – Classification of the images by converting the image into meaningful components for a better analysis such as global histogram segmentation.

➢ Object measurement – Analyzing the analog property of the original scene from the digital image data

➢ Graphic generation – Portraying the solutions obtained in a simple and understanding manner on a display
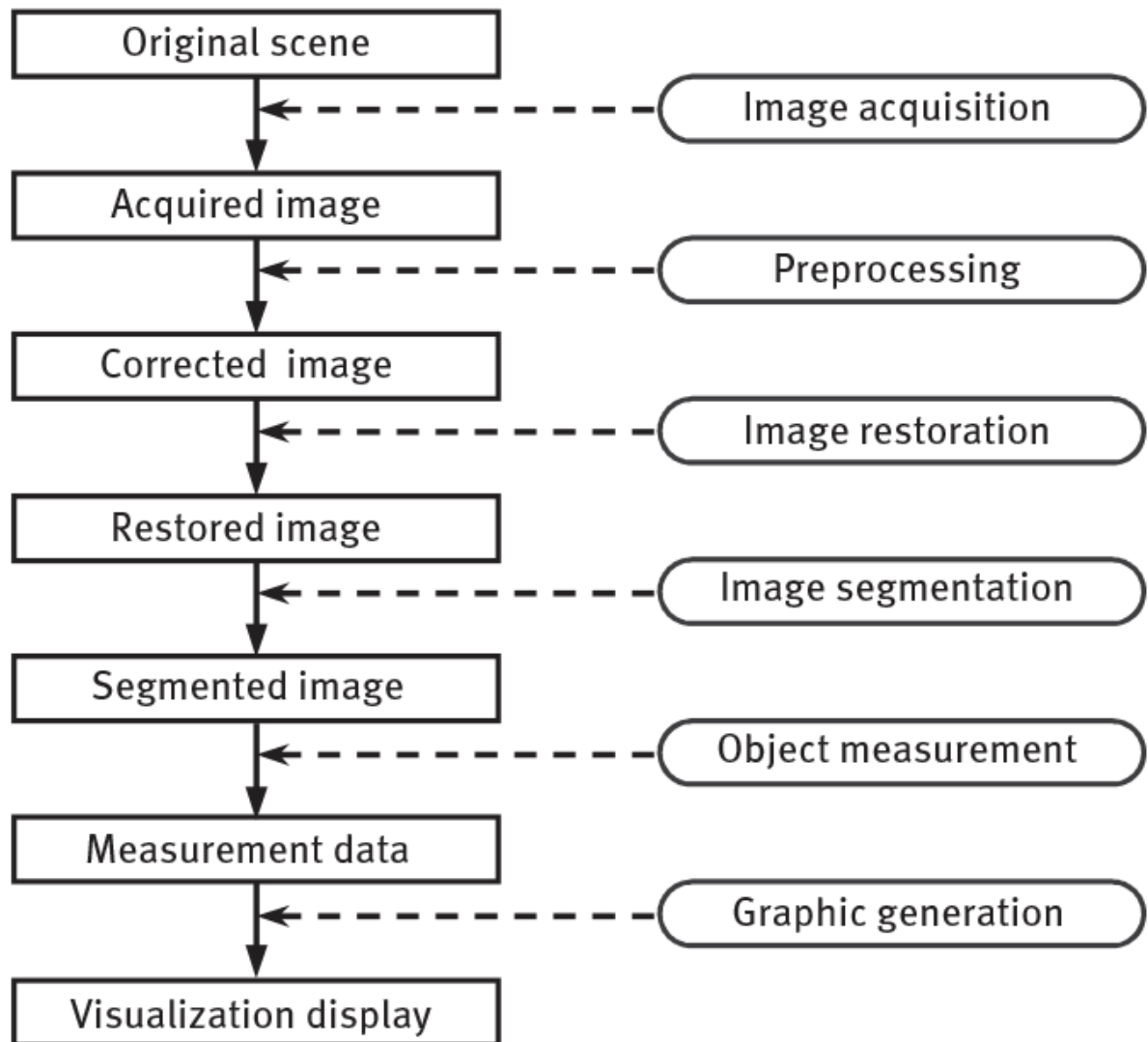
Figure 10 - Flowchart of the Automated Image Analysis [15]

The possible errors with the automated image analysis come when sample preparation quality is not fine, operator bias in setting the parameters and settings, quality of the equipment used as a source of images and the instrument errors or when the assumptions based on stereological formulas turn out to be invalid [16]. During the sample preparation, the samples should be polished with the least relief so that the desired constituents are retained. During the grain size measurement, most of the errors occur due to the improper etching and the downscaling of grains that intersect the frame border [16]. Low KV accelerating voltage and ET detector should be used for etching.

Some important aspects in the analysis of an image are that edge detection is an important aspect because there exists a change in the threshold between the resin and the sample, analyzing the shape, movement, texture, colour, shape and the necessary characteristics [15], positioning and identification of the image automatically which in return saves a lot of lead time.

When the manual measurements and the automated image analysis provides similar material classifications, but computer-aided analysis provides consistent results [20]. Computer-aided analysis requires some knowledge on the parameters to be set and might as well take some time but once the algorithms are set, tested and approved it could be used for several other samples. Hence it provides good repeatability with high accuracy. While in the case of manual measurement it shows overestimation at some regions where the automated analysis cannot detect and estimate. They portray low repeatability and low accuracy because of human fatigue.

2.7.2.1 Materials Image Processing and Automated Reconstruction (MIPAR) [21]

It is an image processing software developed in MATLAB's matrix processing algorithms. It has five modules for selection that is image processor, batch processor, and real-time processor, preprocessor and 3D toolbox as shown in Figure 11 . An image processor is used for creating recipes by utilizing different filters, histogram, segmentation, mathematical equations and measurement on a single image to test the recipe and alter it according to the necessary objective. Batch processor is used when there exist multiple images that need to be tested utilizing the same recipe. The real-time processor works with the same principle of the batch processor, but it acts like a network storage drive such that it is processed in real-time while acquiring the images and gets saved to the directory selected. Postprocessor is used to review the results obtained from the batch processor or real-time processor. The user can access it and optimize the results if they are not satisfactory. The 3D Toolbox is used for visualizing, editing, rendering and animation.
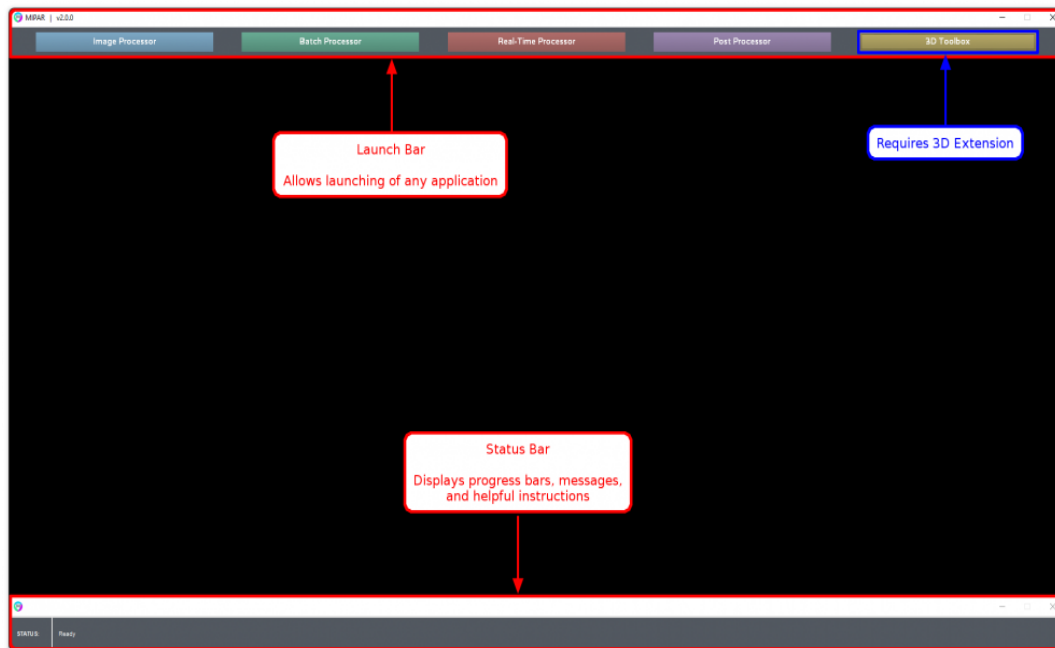
Figure 11 - MIPAR software

The filters used in MIPAR are as follows

- ➤ Median filter – Helps to reduce sparse noise. Each pixel in the image is set to be equal to the median value of its specified neighborhood. It is useful to remove granular noise while maintaining clean feature boundaries. Increase the size of the window value to remove larger artifacts.

- ➤ Wiener filter – It helps to reduce sparse noise and also helps to preserve edges. Pixels present near to the edges uses smaller neighborhood sizes

- ➤ Non-local means – It helps to reduce the noise on the image utilizing an advanced filtering algorithm. The local window of each pixel is compared to the neighboring windows and is averaged depending on the variations. It has two options, window size and strength among which strength should be decreased for low-resolution images

- ➤ Gaussian blur – It helps to blur the image by setting each pixel equal to the average value of the mentioned Gaussian neighborhood pixel. They come in use for removing small artifacts to threshold larger features in the image.

- ➤ Sum filter – It sums the pixel value of the selected neighborhood of a particular pixel.

➢ Grayscale Dilate – This helps to set the pixel to the maximum pixel value in the required neighborhood

➢ Greyscale erode – As the name suggests, it functions opposite to the grayscale. In this, it helps to set to the minimum pixel value in the required

➢ Std. dev filter – It helps in highlighting the edges by brightening pixels having dissimilar neighbors. Each pixel is equal to the standard deviation of the pixels in the mentioned neighbors. Window size is increased to overpower small artifacts, decrease to maintain an accurate feature edge.

➢ Entropy Filters – It functions similarly to standard deviation filter but in this, each pixel in the image is the entropy of the pixel values that is the measure of disorder within the mentioned neighborhood.

➢ Gradient filter – It will set each pixel in the image inversely proportional to the average gradient magnitude of its mentioned neighborhood.

➢ Highlight lines – It uses frangi filter to highlight the linear continuous type features in the image. It has two types, dark and bright. Dark is used to highlight dark linear type feature and the bright type uses bright linear type features. This is useful while detecting continuous lines in the image, but the noise should be decreased before applying this filter.

➢ Bright texture – It highlights the bright components of image textures. It computes grayscale dilation and grayscale erosion is simultaneously known as a top-hat filter then subtracts the result from the image. It is useful to eliminate large, overexposed regions in florescence imaging

➢ Dark texture – It highlights dark components of the image texture. It computes grayscale erosion and grayscale dilation of the image simultaneously known as a bottom-hat filter.

➢ Sharpen – It helps to sharpen the image by deconvolving an unsharpening kernel out of each pixel. It is useful to apply on images which have dulled features due to noise removing filters.

➢ Frequency filter – It modifies the Fourier transform of the image with the existing filters. It is used to background removal to edge finding to artifacts reduction.

➢ Grayscale interpolation – It reconstructs the missing pixels utilizing the average of the known pixels within the mentioned neighborhood. It has two types,

mean and median. Mean used mean of the known pixels within the mentioned window and replaces the unknown pixels and the median used of the known pixel within the mentioned window and replaces the unknown pixels. It consists of two types of iterations, single and complete. Single iteration interpolates the missing pixels once through the image and the complete iteration interpolates missing pixels until there isn't any left in the image.

2.7.2.2 Image J

It is an image processing and analysis software developed based on Java as shown in Figure 12. It is the most widely used image analysis software because it is an open source software and its efficient features. It has limited features in it which is useful for research perspective. Initially scale is set from the scale bar of the image by the software calculating the number of pixels. The image is converted to a suitable type for applying the threshold. Based on the results to be obtained the threshold is set with a suitable filter. To obtain the results, the required results should be selected from the analyze particles option. There is no possibility of going back to the previous step once the threshold is set. The whole process should be repeated from the beginning, but the scale can be used for all the images by selecting global option while setting the scale only if all the images to be examined are of same scale. If there exist multiple images with the same scale, Macro option can be used. In Macro, initially the whole process starting from setting the scale to obtaining the results should be recorded and saved which acts like a recipe followed for other images. It is a very useful software utilized in many different applications such as material science field, medical laboratory field etc.
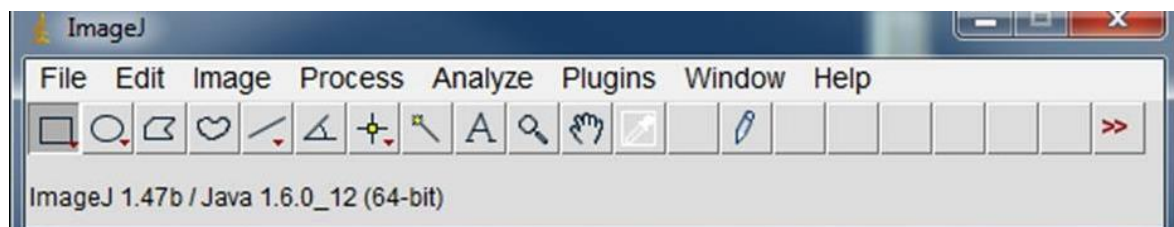

Figure 12 – Image J software

3   Experimental Procedure

In this Master thesis, Ni-based superalloy Haynes 282 is investigated. It has been hot isostatically pressed and fully heat treated leading to an equiaxed microstructure for grain size measurement. Initially, the general material preparation steps have been followed such as cutting the sample along the required direction, mounting, grinding and polishing. The material has been cut along the direction of the build as well as 90° to the direction of build in case of the grain size measure objective(Figure 13) whereas, it has been cut along the direction of the build in case of defect analysis objective (Figure 14).
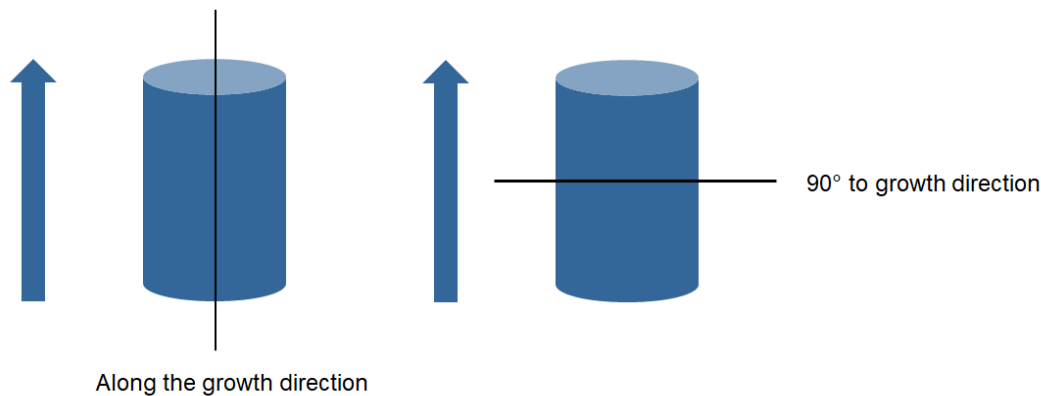

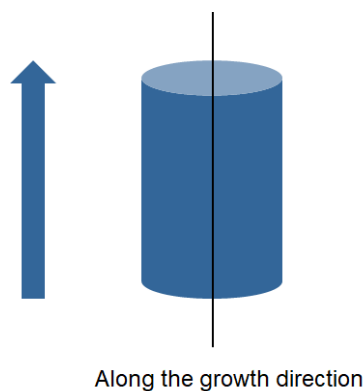**Figure 14 – Grain size measurement objective**

Figure 13 – Defect Analysis Objective

After following the sample preparations steps, the samples were tested for defect analysis. In the case of grain size measurement, four different etchants were used after

completing the sample preparation steps before it's been observed under the microscope. In the previous experiments, it was always difficult to find a good etchant because all the grains were not revealed due to lack of directional heterogeneity and presence of discontinuous grain boundaries. Hence four etchants were tested to find the best etchant.

The four etchants used are as follows: -

> ➢ Diluted Oxalic Acid
> ➢ Kallings Swab
> ➢ Kallings Electro Etch
> ➢ Hydrogen peroxide + HCl

Samples prepared for both the objectives (defect analysis and grain size measurement) are observed under the microscope and images are captured for obtaining the results.

3.1   Microscopy

LOM is used to observe and capture images of the samples. In case of defect analysis objective, 15 samples were tested. A stitched image was captured for all the samples to get an overall view of the sample with 50X magnification. These stitched images were used for manual measurement of defects while the individual images from the stitched image were used for the automated measurement of the defects.

In case of grain size measurement, a single sample is measured with four different etchants. The number of images captured include five images each at 100X, 200X and 1000X magnification respectively for all the four etchants.

3.2   Defect Analysis

Defect analysis is performed manually to set a benchmark and then tested on both the Automated image analysis software to judge the accuracy of the results obtained from the software.

Manual measurement is measured using the NIS software ([Nikon | Healthcare Products & Solutions (Microscope Solutions) | Imaging Software](#)). In this application it was determined that 1,5mm from the surface will be machined away. Hence it is necessary to create a region of interest and measure the defects (porosity and lack of fusion) within the region of interest. Using tools in the NIS software, diameter of the porosity and the

length of potential lack of fusions are measured. In general, Caliper diameter is considered as a measuring element, porosity is measured by drawing a circle over the pore and lack of fusion is measured by drawing the longest diameter within the defect as shown in the Figure 15. After performing many tests, it was determined that defects measuring below 0,03mm were negligible and need not be considered in the defect analysis measurement. Hence the defects above the mentioned range were considered.
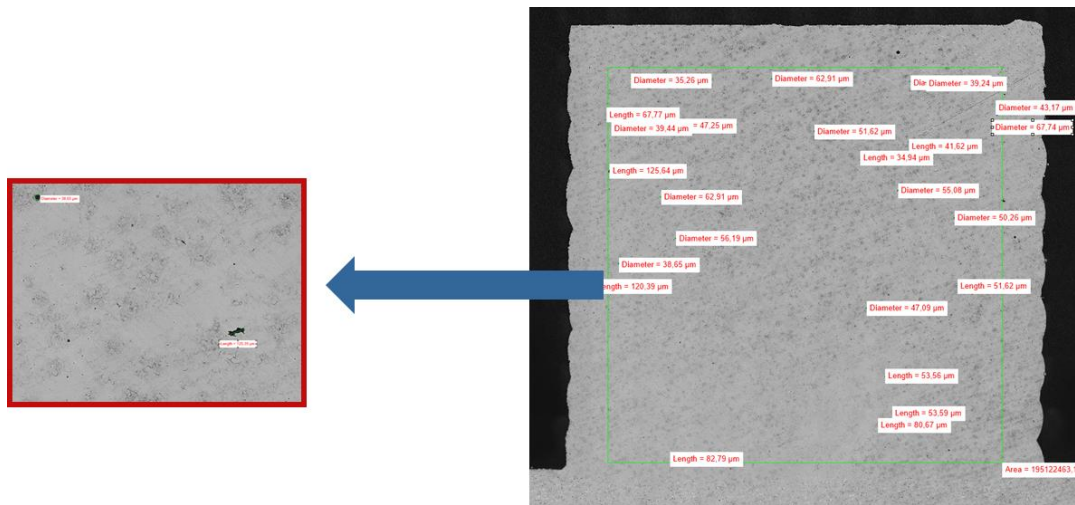
Figure 15 – Manual measurement of defect Analysis

Automated measurement is measured using a recipe which is a step by step procedure performed in the software to obtain the results. The Recipe in MIPAR consists of the following steps as shown in the Figure16
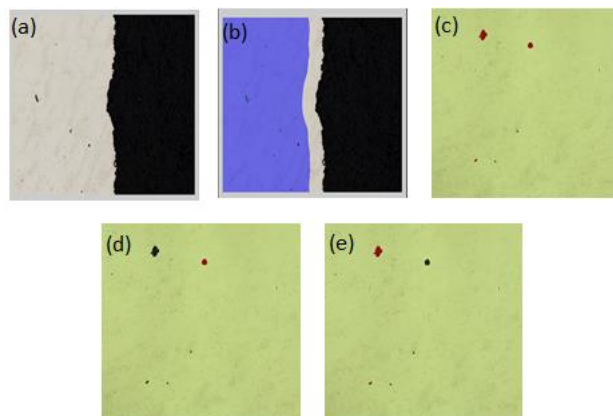

Figure 16 – MIPAR recipe

(a) Surface averaging and basic thresholding is performed initially

(b) As mentioned above, 1,5mm Region of interest was created depicted in the blue area

(c) Detecting all the defects measuring beyond 30µm caliper diameter

(d) Porosity defect is identified using aspect ratio= 1 (1 representing a perfect circle)

(e) Melt defect is identified by considered defect other than porosity defects from the step (c)

The recipe used in Image J software is called macro. In case of Image J there is no possibility to measure both porosity defect and lack of fusion defect in a single recipe. Hence, two different recipes are used with different aspect ratio to differentiate between porosity and lack of fusion. It gives the results in terms of area of fraction. It consists of different steps as shown in Figure 17.

(a) Converting the image to an 8bit image

(b) Setting a suitable threshold such that all the defects are identified

(c) For porosity, Particle size: $0{,}707mm^2$ – infinity and circularity (aspect ratio) = 0.65-1

(d) For Lack of fusion, Particle size: $0{,}707mm^2$ – infinity and circularity (aspect ratio) = 0.00-0.65.
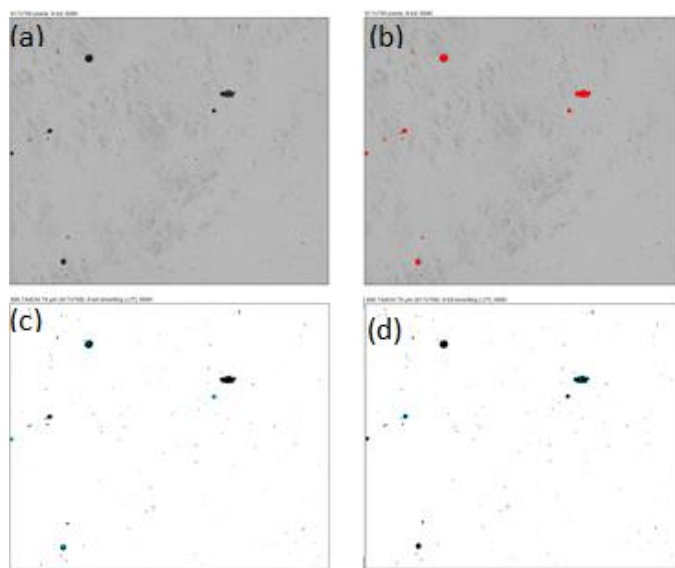

Figure 17 – Image J recipe

3.3 Grain size measurement

Grain size measurement is performed manually to set a benchmark and tested on the automated image analysis software to judge the accuracy of the results obtained from the software.

Average grain size measurement is measured using the ASTM standard E112-12 and ISO 643 standard used for casting and forging because a standard is not approved yet for additive manufacturing. Intercept method was chosen for this application. ASTM Grain size number (G) is defined as $NAE = 2^{G-1}$ where NAE is the number of grains per square inch at 100X magnification.

The average grain size is measured by drawing a line from one side to another side in the image and counting the number of grain boundaries intercepting with that line as shown in Figure 18.

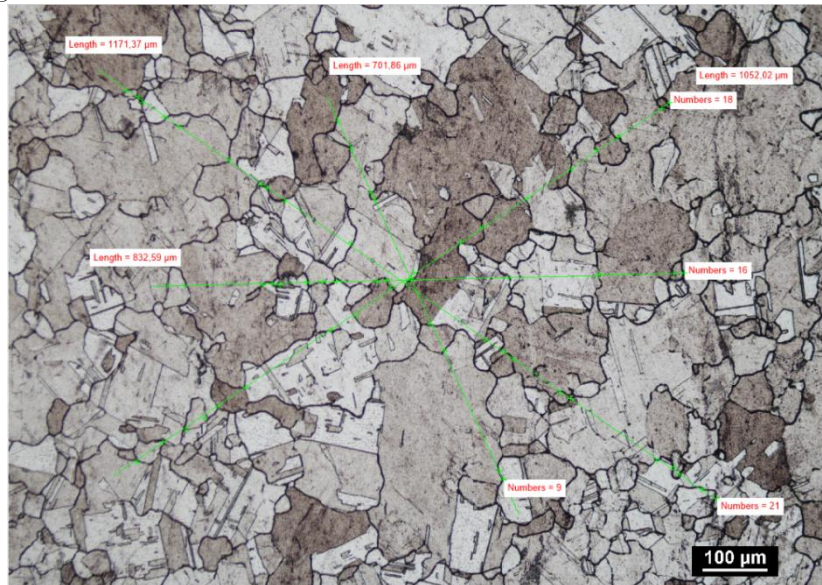**Figure 18 – Intercept method for average grain size measurement**

Average intercept is calculated using the formula $l = \dfrac{L^{Total\ Length}}{Total\ number\ of\ intercepts}$

Average grain size number with the intercept method is determined by the relation in equation (c)

$G = -6{,}6457 \log l - 3{,}298$ ---------(c)

The results were tabulated and measured for each sample using the calculations shown in Table 4.

Table 3 – Intercept method for Average grain size measurement

Length	n	l	G
1000,37	22		
1000,02	19		
832,59	16		
701,86	10		
3534,84	67	0,052759	5,193244

As mentioned before there is no standard for additive manufacturing yet. Hence the results obtained from the grain size measurement is equated in the Hall-Petch equation to obtain the theoretical yield strength results. Hall-Petch equation is considered as a suitable model because it predicts that as grain size decreases, yield strength increases [22].

Hall-Petch equation (d) is

$$Theoretical\ yield\ strength\ (\sigma_y) =\ \sigma_0 * \frac{K_y}{\sqrt{d}}\ \text{------------(d)}$$

Where

σ_0 = Resistance of lattice to dislocation motion (21.8 Mpa).

K_y= strengthening co-efficient (0.158 MPa m$^{1/2}$).

d = Average grain diameter.

After performing several tests, it was determined that yield strength is approximately 600MPa. Hence, 600MPa is considered as a reference value for it to be well in range. Automated image analysis was performed with MIPAR using a grain size measurement recipe as explained in Figure 19
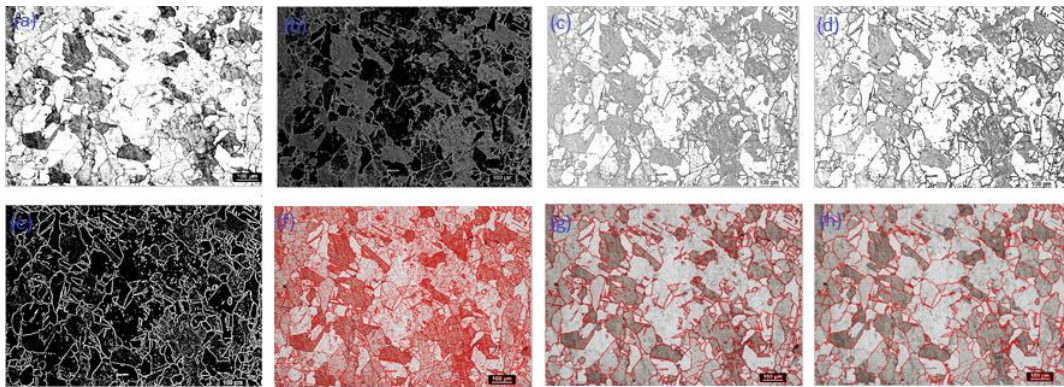
Figure 19 – MIPAR recipe for average grain size measurement.

(a) Initially, contrast is adjusted appropriately.

(b) Standard deviation filter is applied.

(c) The results obtained from the standard deviation filter is inverted.

(d) Contrast is adjusted so that the grain boundary lines are highlighted.

(e) A function called as highlight lines is used.

(f) Adaptive threshold is applied.

(g) Features inside the grains are rejected using Reject features function.

(h) Clean boundaries option is used to get a clear grain boundary marked.

4   Results

The results section presents a detailed and objective description of the results obtained from the experimental work done as explained in section 3.

4.1   Defect Analysis

Defect analysis was carried out using two different parts

4.1.1   Part 1 – To determine the potentials of the automated image analysis software MIPAR and Image J

In this part five images were tested. Manual measurements are set as benchmark to assess the automated image analysis software with calliper diameter as a measuring medium as shown in the Figure20
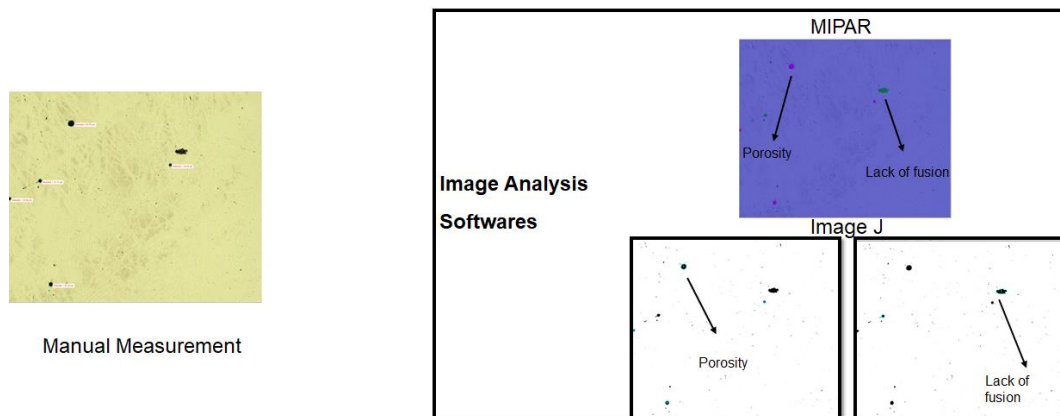
Figure 20 – Defect Analysis measurement.

Caliper diameter cannot be achieved directly in the basic software of ImageJ. It is equated from the Area of the defect with the equation caliper diameter = $\sqrt{((Area * 4)/\pi)}$. By this equation, caliper diameter results of the porosity defects can be equated because it is a perfect circle. It cannot be equated in case of a lack of fusion defect because it is not a perfect circle. Hence, Porosity defect is considered for comparing manual measurement, MIPAR measurement and ImageJ measurement. The results for the porosity defect analysis for the five images considered is shown in Figure 21.
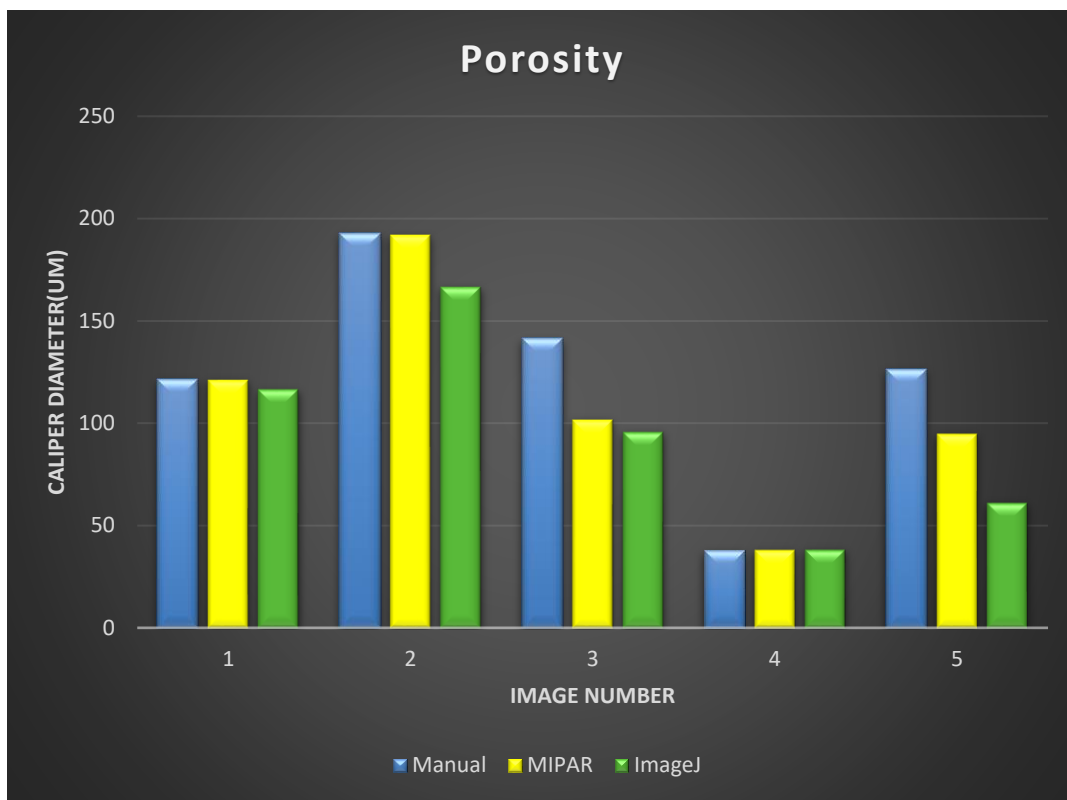
Figure 21 – Porosity defect analysis plot.

4.1.2 Part 2 – To evaluate the results for batch processing of multiple images in MIPAR.

MIPAR was chosen for this part because it was more suitable the application considered in this thesis. In this part, fifteen samples are tested and compared with the manual measurements as the benchmark. The manual measurements were performed with the

Figure 22 – Stitched image of the en-tire sample.

stitched images of the whole sample and the automated image analysis is done with individual images of the stitched images as shown in Figure 22.

The total Caliper diameter was measured for all the fifteen samples. The total Caliper diameter results and the difference between the manual measurement and automated image analysis measurement with the benchmark as manual measurement is plotted as shown in Figure 23. The results for the difference plot is plotted in Figure 24 are calculated using the equation (e)

$$Difference = \frac{Mipar\ measurement\ reults - Manual\ measurement\ results}{Manual\ measuremenet\ results} \text{-----------(e)}$$
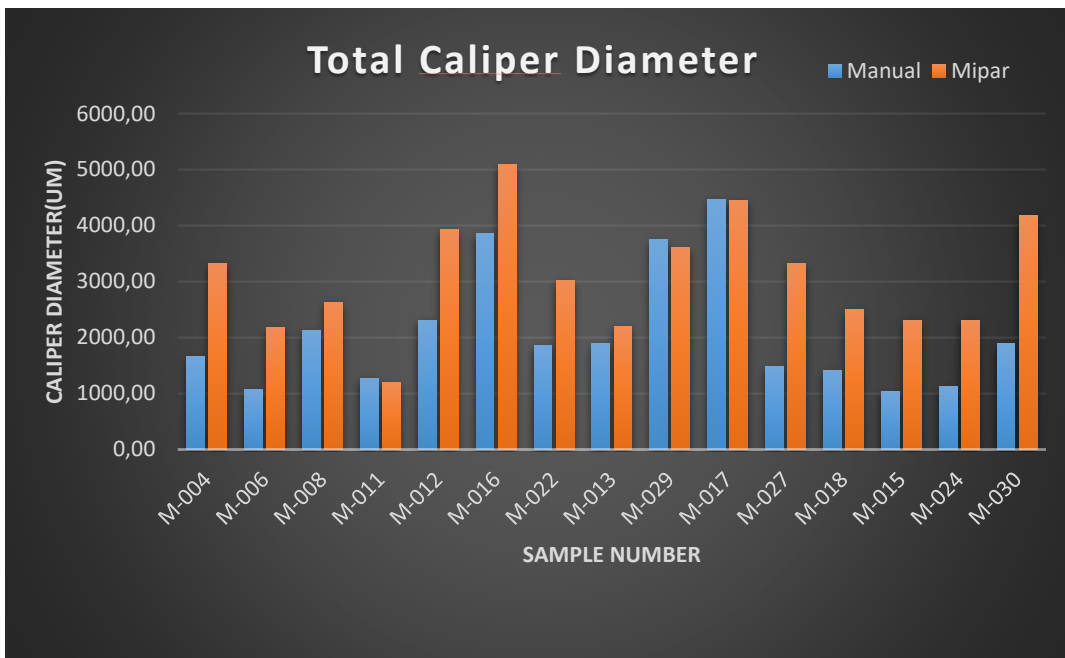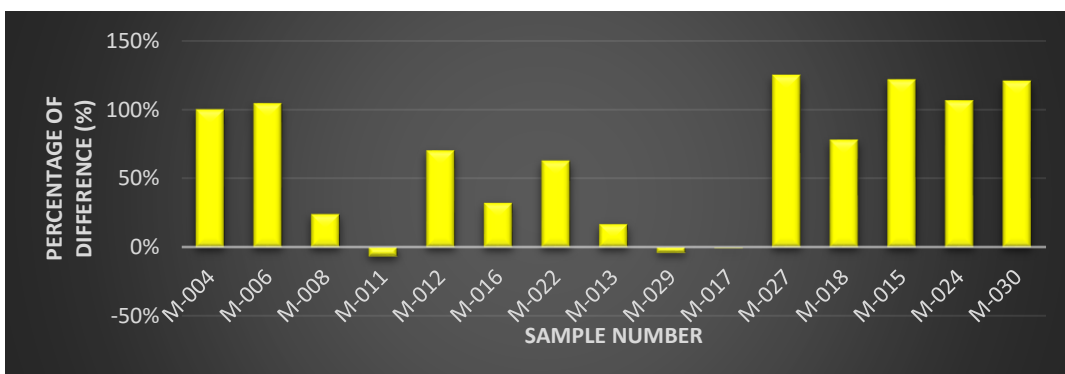

Figure 23 – Total Caliper diameter plot

Figure 24 – Percentage of Difference plot for the total Caliper diameter

As observed in the Figure 22, when each image from the stitched image has been tested there is a possibility for the software to measure the same defect twice which are on the

edges of two images. To overcome this error in the measurement, it was assumed that calculating defect density is the best approach based on the nature of the batch processing with the Caliper diameter results. It is also possible to get results for the overall sample by this approach. Defect density is measured using the equation (f)

$$Defect\ Density = \frac{Total\ Caliper\ diameter}{Area\ of\ Region\ of\ Interest}. \text{----------- (f)}$$

The defect density was measured for all the fifteen samples. The defect density results and the difference between the manual measurement and automated image analysis measurement with the benchmark as manual measurement is plotted as shown in Figure 25. The results for the difference plot are shown in Figure 26 which is calculated using equation (g)

$$Difference = \frac{Mipar\ measurement\ reults - Manual\ measurement\ results}{Manual\ measuremenet\ results} \text{---------- (g)}$$
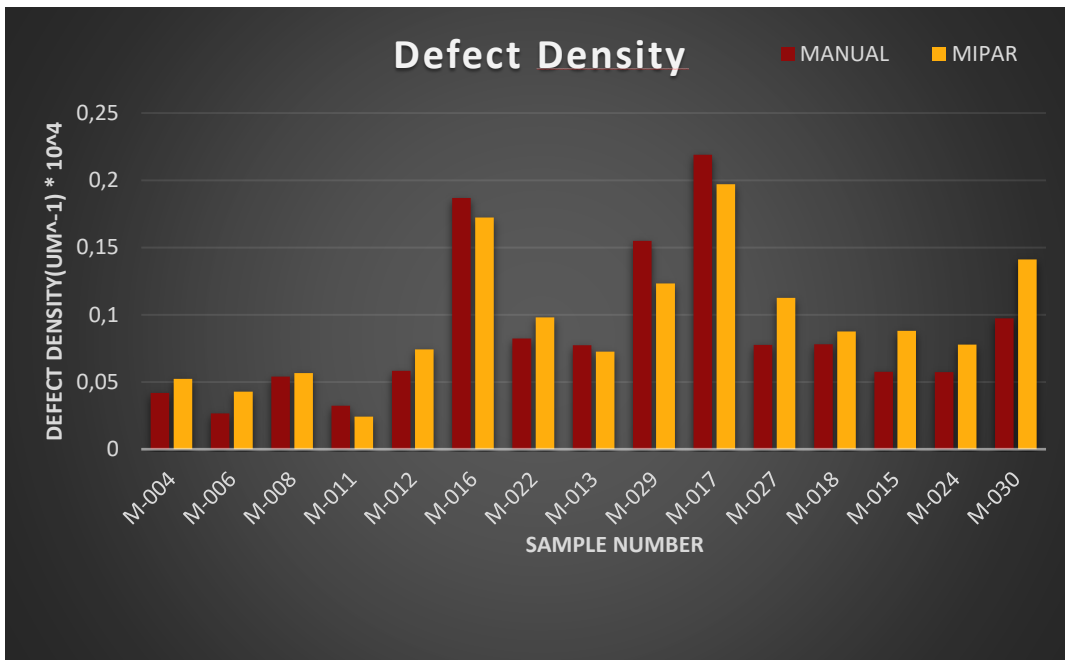
Figure 25 - Defect density plot
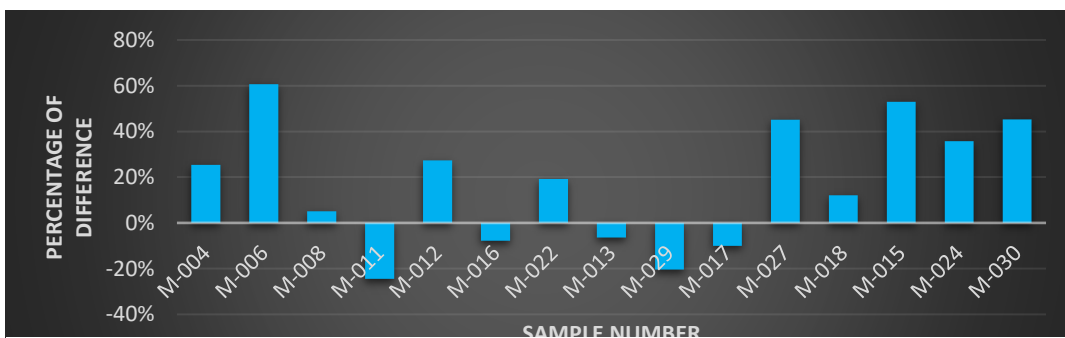
Figure 26 - Percentage of difference of defect density

While comparing the results of manual measurements and automated image analysis measurements, it is also necessary to keep track of the lead time taken from the start till end of the measurements. Figure 27 shows the plot of the lead time taken for manual measurement and the automated image analysis measurement by MIPAR. It can be observed that manual measurement takes longer lead time than MIPAR. Also, the time taken by the manual measurement should be dedicated completely for the measurement while in case of MIPAR measurements other tests could be done parallelly because it is an automated process. There is a possibility for MIPAR to function faster that the current lead time if it is run in a computer with powerful specifications.
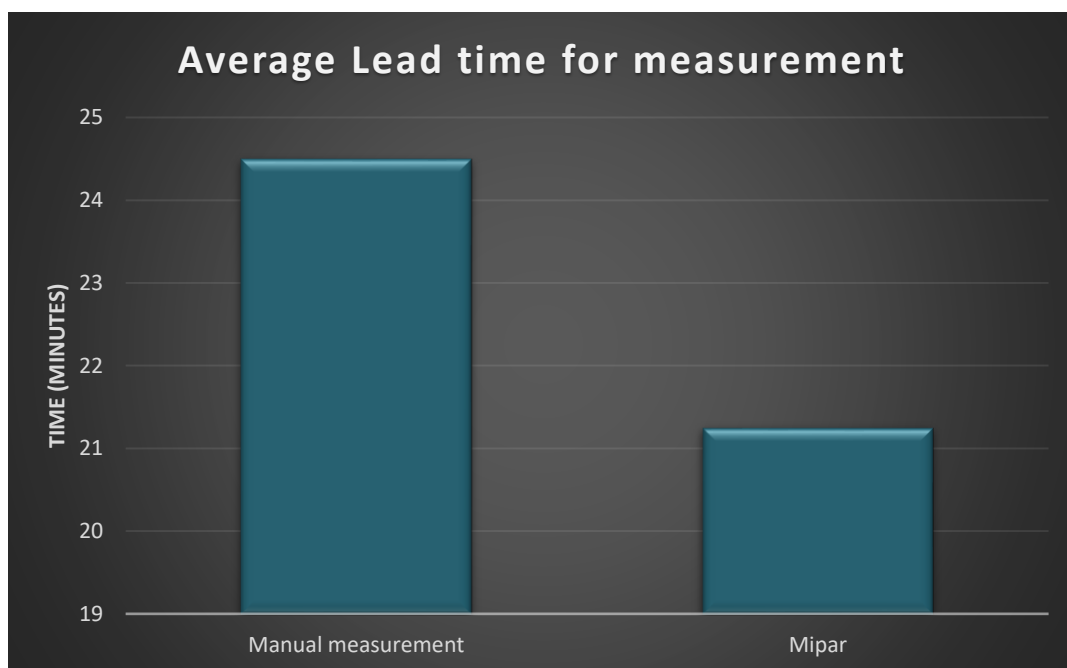
Figure 27 – Average lead time for measurement

4.2   Grain size measurement

Grain size measurement is measured along growth direction and 90° to growth direction as shown in Figure 28 and Figure 29 simultaneously. The images show the results
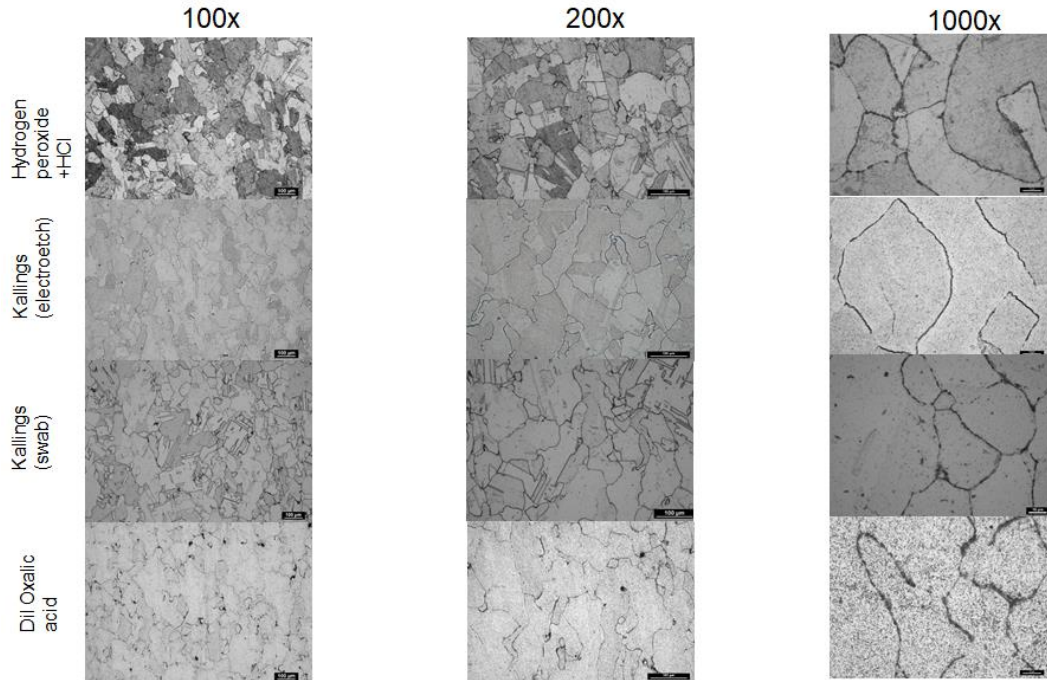
Figure 28 – Images of four different etchants along the growth direction

of the etchant on the same sample in three different magnifications 100X, 200X and 1000X respectively for a better picture of the sample to assess which etchant would reveal the grains appropriately. It is very important for the grains to be revealed evidently for the automated image analysis measurement.
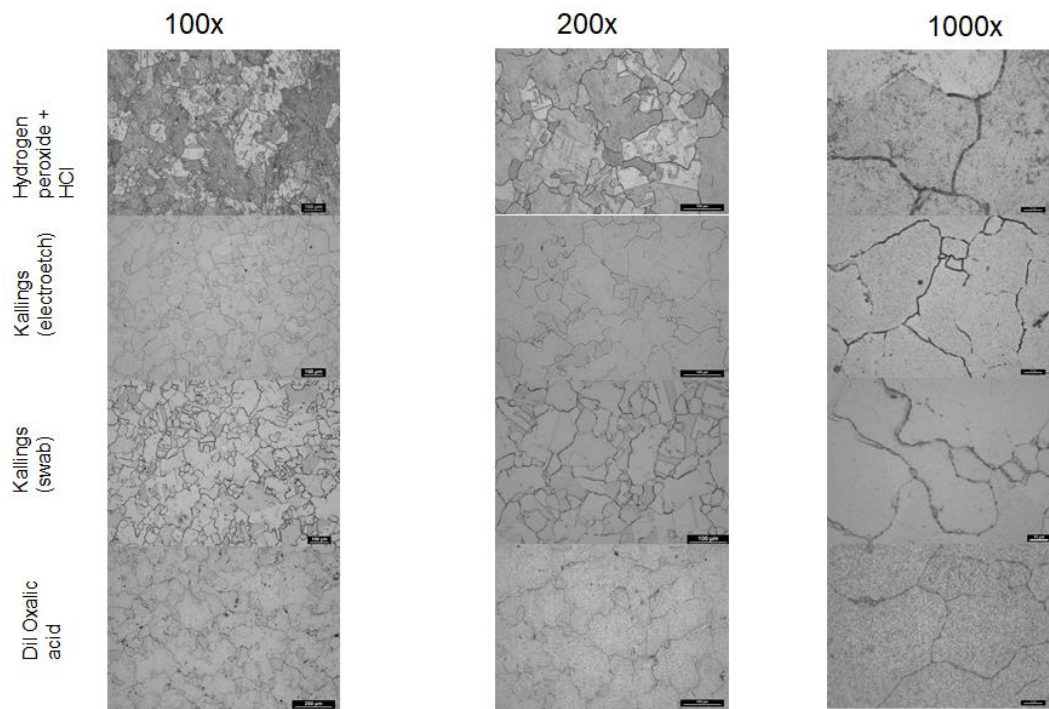
Figure 29 – Images of four different etchants along 90° to growth direction

The images were measured manually which was considered as a benchmark and was compared with the results obtained from the MIPAR measurements. Figure 30 shows the manual and MIPAR measurements of the same image for two different etchants. The grain size measurement results and the difference between the manual measurement and automated image analysis measurement with the benchmark as manual measurement is plotted as shown in Figure 31. The results for the difference plot are calculated using the equation (h).

$$Difference = \frac{Mipar\ measurement\ reults - Manual\ measurement\ results}{Manual\ measuremenet\ results} \text{--------(h)}$$
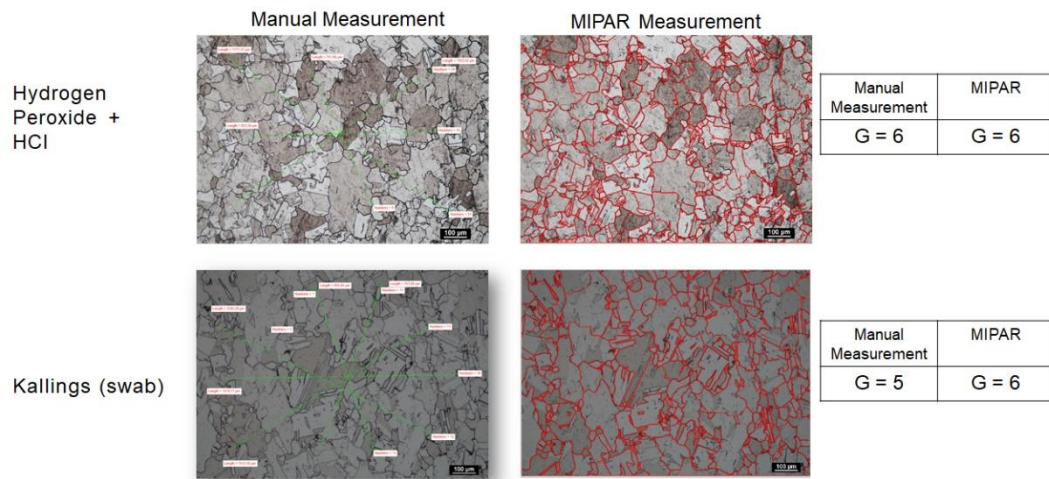
Figure 30 – Grain size measurements of Manual measurement and MIPAR
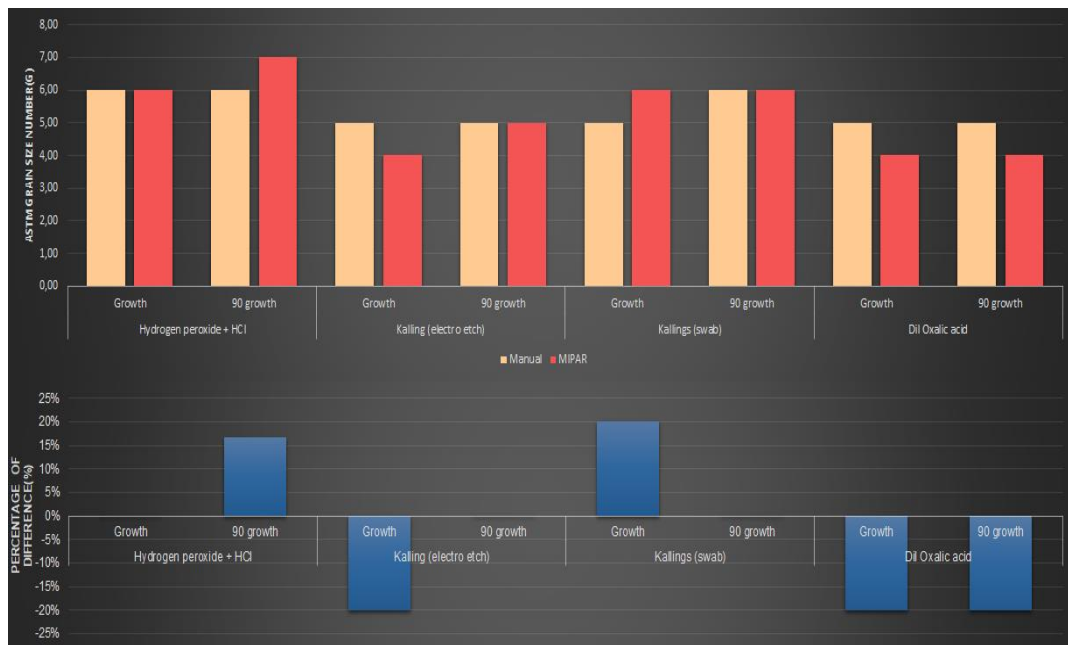
Figure 31 – Grain size measurement

5   Discussion

This section concludes the results and findings. The purpose is to discuss and analyse the meaning of the results related to the theoretical framework, related works and methodology.

5.1   Defect Analysis

Defects in the material have a detrimental effect on the mechanical properties of the material. In this thesis, it was required to measure defects on the sample with a region of interest. It was also necessary to consider the defects which are above the acceptable range. For the applications in aerospace industry it is important to reduce the lead time while not sacrificing the quality of the material. The best approach to save time in the metallography by replacing manual defects measurement is image analysis approach. Two image analysis software MIPAR and Image J were used to determine a better software. Part 1 explains the results obtained from manual measurement, MIPAR measurement and Image J measurements. Part 2 explains the testing of the recipe on the batch processing that is multiple images. As it is explained in section 4.1.2 the individual images were saved from the stitched image because it is not possible to input a large, stitched image directly in the software. These individual images are tested in batch processing with a single recipe because all the images were taken with the same magnification.

5.1.1.   Part 1 – To determine the potentials of the automated image analysis software MIPAR and ImageJ

As explained in section 4.1.1, five images were tested in MIPAR and ImageJ keeping manual measurements as a benchmark. Since it is discovered that MIPAR provided a detailed analysis on the defects such as the volume fraction, caliper diameter of both the defects porosity and LOF whereas on the other hand by the nature of Image J that it can only provide results for volume fraction of the defect and not the Caliper diameter. Lack of fusion cannot be compared because it cannot be equated with the volume

fraction results. Hence, in part 1 the results of porosity measurements were compared to determine the potentials of the image analysis tools.

From Figure 21 it is observed that image number 1, 2, 4 showed a good trend of approximately similar results in manual measurements, MIPAR measurements and Image J measurements while image number 3 and 5 show a difference in measurement with image analysis software compare to the manual measurements. Hence, image 3 measurement was chosen to assess why there was a difference in measurements. It is observed in figure 32 that when the same image was tested in three different measuring mediums. The manual measurement shows that two pores were identified but since there is a small scratch over one of the pores, it has not been considered as a pore by either of the software. It was found that the quality of the image plays a very significant role because the software finds it a difficult task to identify features.

| Manual Measurement | MIPAR | Image J |
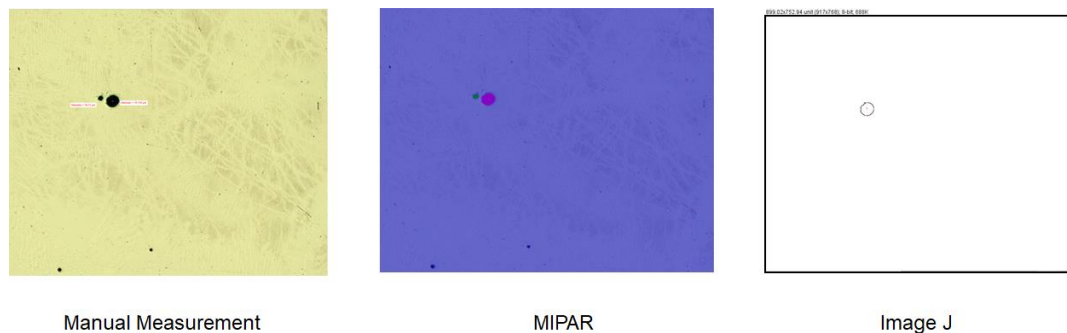
Figure 32 – Porosity measurement of image number 3

For the next part with batch processing MIPAR was chosen as a better option over ImageJ because it portrays more advantages than a basic ImageJ software. It has the ability to provide the results of caliper diameter directly, results of lack of fusion and it also has an added advantage that is at some instances scratched are considered as a defect which can be refined using post-processing function in MIPAR.

5.1.2.   Part 2 – To evaluate the results for batch processing of multiple images in MIPAR

As explained in section 4.1.2, fifteen samples are were used. Manual measurements were performed with the stitched images and the MIPAR measurements were performed with the individual images from the stitched image using batch processing function. Figure 23 shows the total caliper diameter results of both the defects porosity and lack of fusion. The percentage of difference or also known as the error is plotted for comparing the results of manual measurement and MIPAR results. In most of the samples, MIPAR over calculates the total caliper diameter of the defects compared to manual measurements. From the different plots it was observed that M-027 sample had the biggest difference. Hence this sample was looked in detail to check the measurement in MIPAR. As seen in Figure 33 at some instance's scratches were detected as lack of
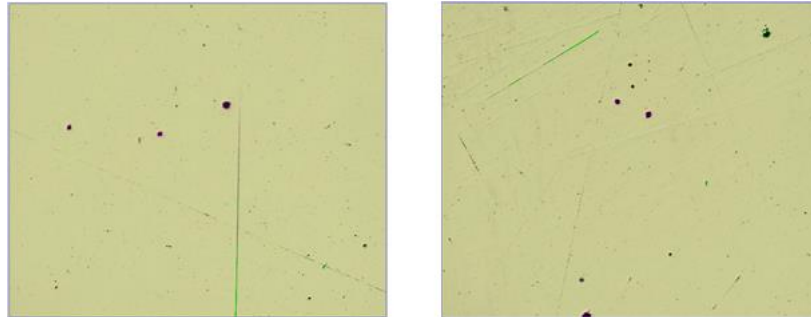
Figure 33 – Images from the MIPAR measurements

fusion. This shows that image quality plays an important role while testing an image on automated image analysis software. These errors can be refined in MIPAR using a function called post processor. In this case post processing was performed on sample M-027 to refine the measurements by omitting the detection of the scratches. The plot of sample M-027 for manual measurement and MIPAR measurement before and post processing is shown in Figure 34.
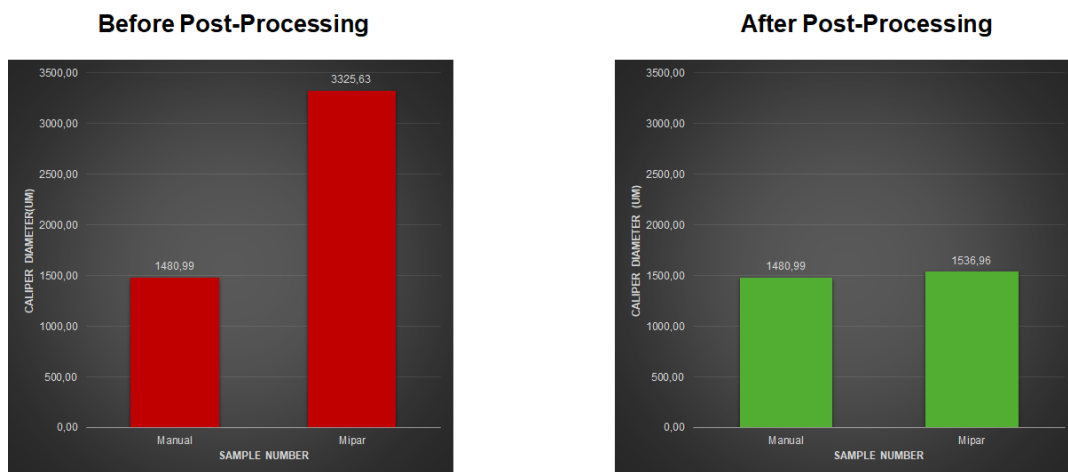
Figure 34 – Plot of sample number M-027

The caliper diameter results vary for the measurement of the lack of fusion by manual measurement and MIPAR measurements because it is the longest diameter in the lack of fusion defect. Hence it is observed that MIPAR over calculates when both the defects are summed up. Few samples also show that Manual measurements calculate more than MIPAR because the region of interest calculated by manual measurements and the MIPAR measurements are different. In few instances, the defects measured by the manual measurement is not considered by MIPAR because it is not in the region of interest set the MIPAR. It is believed that defect above an acceptable range of measurement is critical. Hence after post processing, histogram was plotted for sample M-027 to determine the critical impact of the defects as seen in Figure 35. With help of the histogram distribution of the plot, it is easier to determine the life of the sample.
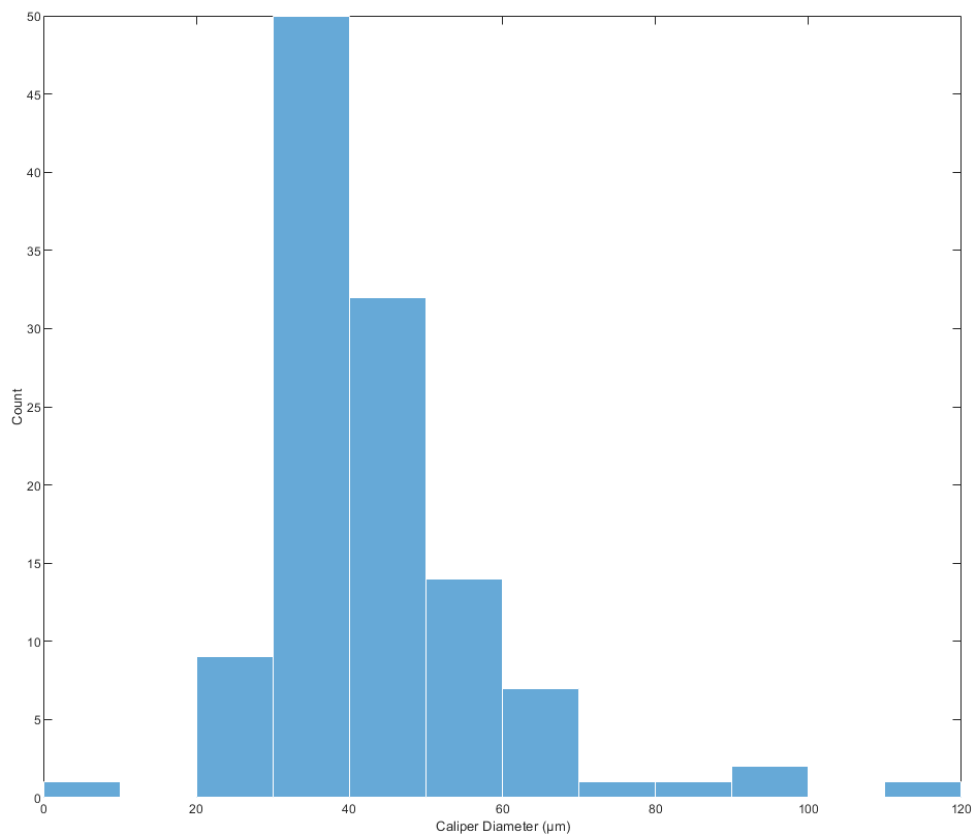
Figure 35 – Histogram distribution of the defects

Defect density was assumed as a best approach based on the nature of batch processing. Like caliper diameter results, percentage of difference or the error is plotted for defect density as well to compare the results of the manual measurements and MIPAR measurements. The difference plots portrayed a varied difference between the MIPAR and manual measurements because at few instances MIPAR over calculates than manual measurements but in a few instances the vice versa happens. The formula of the defect density has the region of interest in place, but as it has been discussed before the region of interest set by manual measurement and MIPAR measurement is different as shown in figure 36. The same defect analysis recipe was also used on different material to check the porosity result and the results turned out to be appropriate.
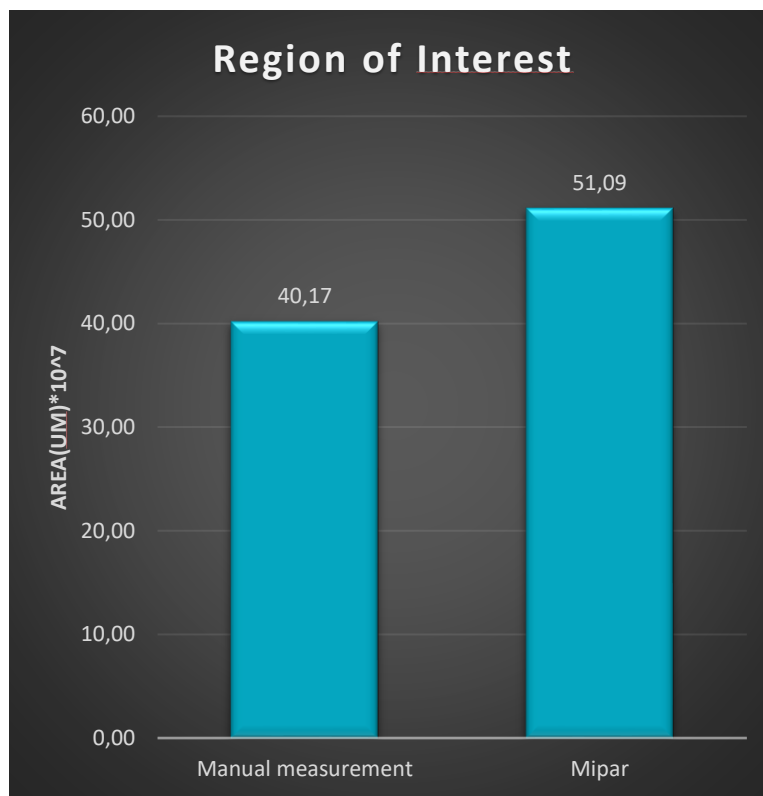
Figure 36 – Region of Interest plot

5.2   Grain size measurement

Grain size measurement is performed with four different etchants as explained in section 3. It is important for the etchants to reveal the grain boundaries evidently for the automated image analysis software to identify the grains. The manual measurement was performed with linear intercept method according to the ASTM standard [17]. The software applies different filters to identify the grains. It was observed that etching solution responds differently on each direction of growth to reveal the grains either because of the material preparation or the ability of the etchant to respond on a single direction. Figure 37 shows the images results of the same etchant in both the direction. It is observed that 90° to growth direction finds it more difficult to reveal the grains.
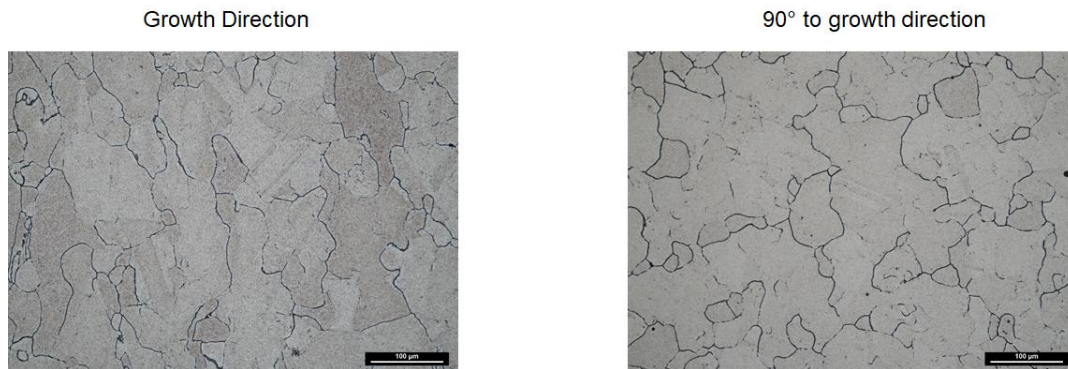
Figure 37 – Etching solution on different growth direction

From figure 30 it was observed that results obtained from MIPAR is approximately equal to the manual measurements which was set as benchmark. But it is explained in section 3.3 that there is no standard set for additive manufacturing yet. Hence Hall Petch equation is used to determine if the measurements obtained could be trusted. Figure 38 shows that the results obtained can be trusted because the results from all the etchants are approximately close to 600MPa.

Figure 38 – Hall-Petch equation plot

Figure 31 depicts the grain size measurements plot for four different etchants at growth direction and 90° to growth direction. The percentage of difference plot explains the

comparison between the manual measurements and MIPAR measurements. MIPAR over calculates the measurements in case of hydrogen peroxide + HCl and Kallings(swab) because the twin boundaries are visible, and the software measures it as grains. While on the other side Kallings(electro etch) and Dil Oxalic acid show that MIPAR measures lesser grains than manual measurements because it is evident from the images of the etchants that these two etchants do not reveal all the grain boundaries clearly for the software to identify. This proves that it is essential to select the best etchant which reveals the grain boundaries evidently. Also, this recipe is critical to be used on different materials because the grain structure is different on different materials. Hence, further optimizations are required to be able to use it for different materials.

It is explained that computer technique provides unique and repeatable results automatically and the time taken is very less [23]. It is evident from the above discussion that Manual measurements usually overestimates the results compare to the results obtained from the image analysis tool.

As mentioned initially, this thesis focuses more on the metallography group to decide if the material clears the level of acceptance regarding the defects and grain size by decreasing the lead time with good accuracy. Automated image analysis is chosen as the best approach to perform defect analysis and grain size measurement keeping the previous approach which is the manual measurement as a benchmark. Manual measurement was found to be time consuming and as mentioned it had a human factor. By human factor it means that the way of measurement by each human varies and another term human fatigue means that after performing the task for more number of samples, humans tend to develop fatigue which will have a direct impact on the results of the analysis. Hence automated image analysis was chosen as a best approach because once the recipes in the software is set and finalized the software always gives the same results even after many tests. Image analysis can be performed in 2D and 3D. Of course 3D analysis will always give good in depth analysis results because of the fact being that each defect could be seen from all the 3 dimensions. By attaining results from 3D analysis, it is easier for the user to decide the impact of the defect on the material and its properties. Whereas, since the cost reduction is one of the main things to be considered and the 3D analysis is an expensive process. Hence, 2D analysis was carried out in this master thesis.

6   Conclusion

6.1   Defect   Analysis

The automated image analysis software demands the best metallography and image quality. While talking about accuracy in case of repeatability, once the recipes built are finalized and approved, it could be used several times still achieving the same results because it is an automated process but in case of manual measurements, repeatability does not exist because of the human factor and human fatigue. With the basic Image J software, it is not possible to measure the caliper diameter because it gives results in terms of area of fraction which makes it impossible to measure and compare the lack of fusion defect. MIPAR gives results for caliper diameter for porosity and lack of fusion directly and it has an added advantage to refine the results using the post processing function. Region of interest calculated by manual measurement and MIPAR were different leading to a difference in the defect density calculation. Histograms showcase the life of the sample by a possibility to have a look at the critical impact.

6.2   Grain size measurement

The HIP and HT condition transformed the grains into equiaxed grains. Etchant solutions hydrogen peroxide and kalling (swab) portrayed good results by revealing the grain boundaries helping the software to identify the grains easily. But a few instances MIPAR over calculated than manual measurement because the twin boundaries were revealed by the etchants which should be optimised in the recipe The response of the etchant to reveal grain boundaries in each direction is different because it was observed that 90° to growth direction found it more difficult to reveal the grains boundaries. MIPAR recipe produced good results with minor optimizations required.

Generalization of the result

To reduce the lead time, it is very important to build good recipes to achieve a quantitative analysis with good accuracy. Image analysis tool MIPAR provided good quantitative results which in return reduces the lead time. In case of defect analysis recipe, the same recipe can be tested on different materials as well. Grain size measurement recipe showed promising results because the results obtained from MIPAR were close to the manual measurement results. Hence, the recipes are good but need few developments to get accurate results.

7   Future Work

➢ Extend the defect analysis recipe in MIPAR to give a condition for Lack of fusion as well like porosity has a condition with the aspect ratio

➢ Develop recipes for measuring other features in the metals such as precipitates, inclusions etc

➢ Develop recipes for different materials

1 References

[1] A. Ganvir and H. Väst, "Microstructure and Thermal Conductivity of Liquid Feedstock Plasma Sprayed Thermal Barrier Coatings Sintering behaviour of 8YSZ suspension plasma sprayed thermal barrier coatings View project".

[2] D. Leidermark, "Mechanical behavious of single crystal Ni-based superalloys," Linköping University, Linköping, Sweden, 2008.

[3] C. Joseph, "Microstructure Evolution and Mechanical properties of haynes 282," Chalmers Reproservice, Götborg, Sweden, 2018.

[4] "Introduction to the special issue on additive manufacturing: Editorial Board of special issue on additive manufacturing," *Engineering,* pp. 1-100, 2017.

[5] " https://www.digitalalloys.com/blog/powder-bed-fusion/ : Access date : 04/03/2020".

[6] M. L. D. M. J. M. A. O. Benjmain Casey Graybil, "Additive Manufacturing of Nickel-Based Superalloys," in *Research Gate*, June 2018.

[7] H. C. G. M. B. R. Gorsse S, "Additive manufacturing of metals: a brief review of the characteristic microstructures and properties of steels, Ti-6Al-4V and high-entropy alloys. Sci Technol Adv Mater.," 2017, 2017; Aug.

[8] M. J. D. S. J. Donachie, Superalloys : A Technical Guide, 2nd ed. Materials Park, OH, 2002.

[9] L. Pike, HAYNES® 282™ Alloy: A New Wrought Superalloy Designed for Improved Creep Strength and Fabricability, 2006.

[10] J.Andersson, "Weldability of precipitation hardening superalloys-influence of microstructure," Chalmers University of Technology, 2011.

[11] W. P. M. W. N. C. G. W. D. Z. a. R. M. P. Adelajda Polkowska, "Microstructure and Hardness Evolution in Haynes 282 Nickel-Based Superalloy During Multi-variant Aging Heat treatment," *Journal of Materials Engineering and performance,* vol. 28, no. 7, pp. 3844-3851, 2019.

[12] Y. l. Q. B. Bi Zhang, "Defect formation mechanisms in selective laser malting : A review," 2017.

[13] M. Neikter, Microstructure and hydrogen embrittlement of additively manufactured Ti-6Al-4V.

[14] E. Hallberg, "Investigation of hot cracking in additive manufactured ni-based superalloy," 2018.

[15] Z. Y. J. B. Zhu, Image Engineering, Tsinghua University Press, 2017.

[16] "Image Analysis," in *Materials Characterization*, ASM International, 1986, pp. 309-322.

[17] "Standard Test Methods for Determining Average Grain Size 1".

[18 G. V. Voort, "Grain size measurement: The Jeffries Planimetric Method,"
]   November 12, 2012.

[19 G. V. Voort, "Grain size measurement: The Heyn intercept method," December
]   14, 2012.

[20 "Standard Test Method for Determining Volume Fraction by Systematic Manual
]   Point Count 1".

[21 J. H. D. W. B. e. a. Sosa, "Development and application of MIPAR™: a novel
]   software package for two- and three-dimensional microstructural
     characterization," *Springer,* p. 123/140, 2014.

[22 Wikipedia, "Grain Boundary strengthening," p.
]   https://en.wikipedia.org/wiki/Grain_boundary_strengthening#CITEREFSmith
     Hashemi2006.

[23 Z. Latal Ca and L. Wojnar, "Computer-aided versus manual grain size assessment
]   in a single phase material".

[24 "Quantitative Image Analysis," in *Metallography and Microstructures,* ASM
]   International, 2004, pp. 403-427.

[25 V. T. Le, H. Paris and G. Mandil, "The development of a strategy for direct part
]   reuse using additive and subtractive manufacturing technologies," *Additive*
     Manufacturing, vol. 22, pp. 687-699, 1 8 2018.

[26 M. N. S. S. B. D. F. Yousub Lee, "Effect of Fluid Convection on Dentrite Arm
]   Spacing in Laser Deposition," *Metallurgical and Materials Transactions B,* March 2014.

A. Appendix – Defect Analysis measurements

Type	Sample	Manual					Mipar					
		Total ROI	Total Caliper	Area	Time(mins)	Defect density	Total ROI	al Caliper(>50	Total Caliper	Area	Time(mins)	Defect density
1	M-004	399217021	1668,35	2186070,747		0,0418	635666202,7	3331,122082	8976,0489	8715072,015		0,052403637
	M-006	401684486,9	1069,04	897589,5591		0,0266	510944873,1	2183,116641	5551,5499	3743206,287		0,042727049
	M-008	393427043,3	2123,79	3542525,821	45	0,0540	463820722,3	2631,751681	5999,1292	5439759,501	35	0,056740709
	M-011	395231577,4	1274,32	1275401,372		0,0322	488595059,7	1189,987	4410,203	1112178,039	15	0,024355281
	M-012	395628024,6	2307,45	4181715,471	25	0,0583	528987704,4	3927,619652	13154,577	1211570,611	25	0,07247844
	M-016	205983051,5	3850,64	11645435,04	20	0,1869	295534016,9	5091,095765	11118,742	2035693,613	15	0,172267674
	M-022	226050272,7	1859,32	2715177,106	20	0,0823	3,08E+08	3024,397	13154,577	7184019,104	20	0,098053635
2	M-013	243641491,1	1886,36	2794724,735	20	0,0774	304033520,4	2204,753569	6800,6402	3817772,013	20	0,072516792
	M-029	241907113,7	3745,68	11019229,43	20	0,1548	292291729,5	3600,331703	6865,1459	1018063,602	20	0,123175969
	M-017	204085338,6	4470	15692962,16	30	0,2190	225423649,6	4444,976	11922,725	1551774,898	25	0,197183215
	M-027	190964007,1	1480,99	1722638,438	25	0,0776	295413453	1536,960806	7439,84	1855305,648	25	0,052027448
3	M-018	180150649,8	1405,35	1551168,145		0,0780	285850119,3	2500	6595,7162	4908738,521		0,087458421
	M-015	181298009,3	1044,36	856624,2025	20	0,0576	262293339,7	2311,383956	5523,426	4195986,383	20	0,088122099
	M-024	195122463,1	1119,3	983972,3367	20	0,0574	296467278,9	2307,449044	7104,7566	4181712,006	15	0,077831491
	M-030	194908374,2	1895,386	2821533,547		0,0972	295811661,5	4177,345	8691,4	1370536,387	20	0,141216373

B. Appendix – Results obtained from Hall-Petch Equation

Etchant	Direction	Theoretical yield strength
Hydrogen peroxide	Growth	568,8512769
	90 growth	509,223226
Kalling (electro etch)	Growth	441,926474
	90 growth	466,14341
Kallings (swab)	Growth	471,7918782
	90 growth	513,03711
Dil Oxalic acid	Growth	423,959094
	90 growth	453,9670571

Results from Grain size measurement

Etchant	direction	Manual	MIPAR
ydrogen peroxide + H	Growth	6,00	6,00
	90 growth	6,00	7,00
Kalling (electro etch)	Growth	5,00	4,00
	90 growth	5,00	5,00
Kallings (swab)	Growth	5,00	6,00
	90 growth	6,00	6,00
Dil Oxalic acid	Growth	5	4,00
	90 growth	5	4,00